North-south Asymmetric Nightside Distorted Transpolar Arcs within A Framework of Deformed Magnetosphere-Ionosphere Coupling: IMF-B_y Dependence, Ionospheric Currents, and Magnetotail Reconnection

Motoharu Nowada[1], Qiu-Gang Zong[2], Benoît Hubert[3], Quan-Qi Shi[1], Yong-Fu Wang[2], Jun Yang[1], Adrian Grocott[4], Alexander W. Degeling[1], An-Min Tian[1], Xu-Zhi Zhou[2], and Chao Yue[2]

[1]Shandong Key Laboratory of Optical Astronomy and Solar-Terrestrial Environment, School of Space Science and Physics, Institute of Space Sciences, Shandong University, Weihai, Shandong, People's Republic of China.

[2]Institute of Space Physics and Applied Technology, School of Earth and Space Sciences, Peking University, People's Republic of China.

[3]Space science, Technologies and Astrophysics Research (STAR) Institute, Université de Liège, Belgium.

[4] Space and Planetary Physics Group, Department of Physics, Lancaster University, Lancaster, UK.

Key points:

1. A new morphological type of transpolar arc, characterized by large nightside distortions in the pre- or post-midnight sector, is described.

2. Nightside reconnection and magnetotail deformation by IMF penetration play essential roles in the formation of nightside distorted TPA.

3. Nightside distorted TPAs can be used as a remote-sensing tool to diagnose globally IMF-deformed magnetospheric processes.

Corresponding Authors:
Motoharu Nowada (moto.nowada@sdu.edu.cn),
Qiu-Gang Zong (qgzong@pku.edu.cn),
Quan-Qi Shi (sqq@sdu.edu.cn)

Abstract

The terrestrial magnetosphere is perpetually exposed to, and significantly deformed by the Interplanetary Magnetic Field (IMF) in the solar wind. This deformation is typically detected at discrete locations by space- and ground-based observations. Earth's aurora, on the other hand, is a globally distributed phenomenon that may be used to elucidate magnetospheric deformations caused by IMF variations, as well as plasma supply from the deformed magnetotail to the high-latitude atmosphere. We report the utilization of an auroral form known as the transpolar arc (TPA) to diagnose the plasma dynamics of the globally deformed magnetosphere. Nine TPAs examined in this study have two types of a newly identified morphology, which are designated as "J"- and "L"-shaped TPAs from their shapes, and are shown to have antisymmetric morphologies in the Northern and Southern Hemispheres, depending on the IMF polarity. The TPA-associated ionospheric current profiles suggest that electric currents flowing along the magnetic field lines (Field-Aligned Currents: FACs), connecting the magnetotail and the ionosphere, may be related to the "J"- and "L"-shaped TPA formations. The FACs can be generated by velocity shear between fast plasma flows associated with nightside magnetic reconnection and slower background magnetotail plasma flows. Complex large-scale TPA FAC structures, previously unravelled by an Magnetohydrodynamic (MHD) simulation, cannot be elucidated by our observations. However, our interpretation of TPA features in a global context facilitates the usage of TPA as a diagnostic tool to effectively remote-sense globally deformed terrestrial and planetary magnetospheric processes in response to the IMF and solar wind plasma conditions.

Keywords: Nightside Distorted Transpolar Arc; Solar Wind-Magnetotail-Ionosphere/Atmosphere Coupling; Magnetospheric Diagnosis; Magnetotail Magnetic Reconnection; Plasma Flow Shear; Field-Aligned Currents

Plain Language Summary

In magnetospheric physics, the aurora is one of the most important phenomena in qualitatively and quantitatively understanding the transfer of plasma and energy from the solar wind to the high-latitude atmosphere via terrestrial and other planetary magnetospheres. To understand the global picture of the plasma supply from the terrestrial magnetosphere, deformed by the Interplanetary Magnetic Field (IMF) in the solar wind, to the auroral zone, the formation process of a new morphology of auroral transpolar arc (TPA) is investigated in this study. The source of these TPAs can be the electric currents flowing along magnetic field lines, induced by the plasma flows in the magnetosphere. The conventional TPA has a straight bar shape, which connects the nightside and dayside of the auroral oval. The new TPA morphologies, on the other hand, have significant “distortions” toward pre- and post-midnight at their nightside ends, which may be caused by magnetic field line twisting and magnetosphere deformations due to the action of the IMF. Our results facilitate a paradigm shift in understanding the implications of TPA structure on global scale dynamics in the deformed magnetosphere, and as such, the usage of the auroral TPA shape as a tool to diagnose global-scale magnetospheric effects.

1. Introduction

The terrestrial magnetosphere, which dynamically changes through interactions with the high-speed plasma streams and Interplanetary Magnetic Field (IMF) originating from the Sun, effectively shields life on Earth from harmful radiation effects associated with these particles (Black, 1967; Glassmeier et al. 2009, 2010; Shi et al. 2013). The geomagnetic field surrounding the Earth also plays a role in preventing the atmosphere from escaping into space (Wei et al. 2014). Therefore, it is important to understand the morphologies and dynamics of our terrestrial magnetosphere, in particular, the processes by which plasma is supplied to, and released from, the magnetotail and transferred to the high-latitude atmosphere or ionosphere.

Significant global magnetospheric effects are produced not only by changes in the IMF north-south component (IMF-B_z) but also its dawn-dusk component (IMF-B_y). A series of observational studies (Kaymaz et al. 1995; Nishida et al. 1995, 1998; Pitkänen et al. 2013, 2015, 2017) have found that under dominant IMF-B_y conditions, the magnetotail (plasma sheet) becomes increasingly twisted with down-tail distance, caused by the penetration of IMF-B_y into the magnetotail. Magnetotail deformation and IMF penetration to the magnetotail have been attributed to magnetic reconnection under dominant IMF-B_y conditions (Gosling et al. 1990; Cowley, 1981, 1994; Grocott et al., 2007; Tenfjord et al. 2015, 2018), which causes asymmetries in the magnetosphere. Inside the deformed magnetosphere, magnetic reconnection can occur and release energized plasma (electrons) earthward and tailward (Petrukovich et al. 1998; Nagai et al. 2001; Angelopoulos et al. 2013; Wang et al. 2020, and references therein). The "source" of auroral arcs, which are frequently seen within the polar cap region (sun-aligned arcs), is considered to be the currents flowing along the magnetic field, carried by precipitating energetic plasma (electrons) (see the details in a review by Zhu et al. 1997). These field-aligned electron flows originate from the magnetotail. When magnetic reconnection occurs in the nightside magnetosphere, magnetic energy stored in the magnetotail is converted to particle kinetic energy, producing accelerated plasma flows out of the reconnection region as earthward and distant-tailward high-speed exhaust jets (e.g., Baumjohann et al. 1989, 1990; Angelopoulos et al. 1992, 1994). As a result, localized fast plasma flows associated with reconnection are conveyed along the field lines, and embedded within lower velocity plasma flows of magnetospheric origin in the magnetotail. Flow shear across field lines between high and low velocity flow regions generates electric currents that flow parallel to magnetic field lines, known as Field-Aligned Currents (FACs) (Hasegawa and Sato, 1979; Birn and Hesse, 1991; Fairfield et al. 1999). Evidence of this process has been compiled by sparse, spatially discrete ground-based, and space-based magnetic field and particle observations (Angelopoulos et al. 1996; Fairfield et al. 1999, and references therein). However, the aurorae seen in the Northern and Southern Hemispheres can be used as a tool to globally diagnose these magnetospheric processes.

A specific auroral form observed under northward IMF-B_z conditions, the Transpolar arc (TPA), occurs at extremely high latitudes. This is identified as a “bar-shaped” emission within the polar cap region, extending from the poleward edge of the nightside auroral oval toward the dayside (Frank et al. 1982). Its formation mechanism and features have been explained in terms of magnetospheric convection and its relationship with the IMF orientation (Fear and Milan, 2012a, 2012b). TPA locations depend on the extent of clockwise or counter-clockwise plasma sheet twisting (viewed from the magnetotail), which is controlled by the IMF-B_y polarity (i.e. either dawnward or duskward, for clockwise or counter-clockwise twisting) (Tsyganenko and Fairfield, 2004; Tsyganenko and Stinov, 2005; Tsyganenko et al. 2015; Cumnock et al. 2002).

The TPA formation model proposed by Milan et al. (2005) is one of the most representative TPA formation models based on nightside magnetic reconnection, and has been applied to explain the developments of many TPAs (Fear and Milan, 2012a, b; Kullen et al. 2005; Nowada et al. 2018). In this model, the TPA growth is attributed to the continual formation of newly closed field lines by magnetotail reconnection, whose location retreats tailward. Several “non-straight” TPAs were also identified in previous statistical studies (Fear and Milan, 2012a; Kullen et al., 2015), which contrast with the “bar”-shaped TPA (hereafter, referred to as a “regular TPA”) previously discussed (Fear and Milan, 2012a, b; Kullen et al. 2005; Nowada et al. 2018). However, neither the physical mechanism for these TPAs, nor their implications on the IMF-deformed magnetospheric dynamics have been discussed.

In this paper, we first identify a new morphological type of nightside distorted TPA, which is distinct from the “regular” TPA. Utilizing space-borne images and in-situ magnetotail observations, together with ground-based geomagnetic field and high-frequency (HF) radar observations, we obtain a global picture of the plasma supply from the deformed magnetotail to the high-latitude atmosphere (auroral zone) by considering the implications of these observations in the nightside distorted TPA formation. In so doing, we demonstrate that the nightside distorted

TPAs can be used as a remote-sensing diagnostic tool for global magnetospheric effects.

2. Instrumentation

New morphological TPAs discussed in this paper were identified using a large database spanning 5 years of auroral observations from 2000 to 2005 by the Wideband Imaging Camera (WIC), which is part of the Far Ultraviolet (FUV) instrument (Mende et al. 2000a, b, c) onboard Imager for Magnetopause-to-Aurora Global Exploration (IMAGE) , launched in March, 2000. IMAGE FUV-WIC imaged the aurora in a broad wavelength range from 140 nm to 190 nm, with a cadence of 2 minutes. From this database, we chose 9 nightside distorted TPAs based on visual inspection, which were clearly imaged in the plots of the IMAGE FUV-WIC data after the removal of dayglow and background contamination, as described below.

The IMAGE FUV-WIC data frequently includes optical contamination, such as sunlight (dayglow) and instrumental optical noise. These non-auroral signals are removed as much as possible from the original WIC images by least squares fitting techniques. The image is separated into two parts along the terminator, but still has an overlap between the dayside and the nightside parts (i.e. the nightside part extends somewhat over the dayside and vice versa). The dayside part of the image is fitted using a two-dimensional Fourier series while the nightside part is fitted using a two-dimensional polynomial. The auroral emission is excluded from the fitting process, and the overlap region is used to produce a smooth merging of both parts. The fitted glow and background are interpolated over the auroral region (including over the transpolar arc region, which is excluded from the fitting process as well). Subtraction of the fitted signal from the images taken and observed over the whole Earth extracts only the auroral signals, albeit with some unavoidable noise contamination. The light from stars, which occasionally appear over the limb of the Earth, can be somewhat scattered and leave their traces on the images. Note that these optical effects are hard to remove, and must not be confused with a real emission from the upper atmosphere. Because non-auroral signals generated by the bright dayglow can only approximately be represented by this method, the optical contamination cannot be completely cleaned from the image. In this study, we discuss the characteristics of unique TPA morphologies, identified based on significant auroral signals, which were extracted through these IMAGE FUV-WIC data processing.

3. Results

3.1 Overview of Nightside Distorted TPAs

"Regular" TPAs generally have a straight shape connecting the nightside and dayside auroral oval. In contrast, all TPAs discussed in this paper have a significant "distortion" at the nightside ends (hereafter, referred to as "nightside distorted TPAs"). Figure 1 shows false color images of 8 representative nightside distorted TPAs, which were identified from IMAGE-FUV-WIC observations. The top (bottom) row of panels correspond to cases of IMF-$B_y < 0$ (IMF-$B_y > 0$), and the first three columns show Northern Hemisphere (NH) observations, while the last column displays Southern Hemisphere (SH) observations. Each panel is oriented such that the top, right, bottom and left sides, corresponding to noon (12 MLT), dawn (6 MLT), midnight (24 MLT), and dusk (18 MLT), respectively. The color scale is expressed in Analogic-Digital Units (ADU), which is proportional to the observed auroral brightness (Mende et al. 2000b). The upper panels (a) to (c) display dawnside TPAs with the nightside ends distorted toward midnight or pre-midnight, observed in the NH. Hereafter, we identify these as "J"-shaped TPAs based on their resemblance to the letter "J". In all observed TPAs, the "J"-shaped TPAs in the NH occur during a negative (dawnward) IMF-B_y interval. The bottom panels (e) to (g) show nightside distorted TPAs with the opposite chirality that occurred on the duskside, in which the nightside ends get distorted toward midnight or post-midnight. We identify these as "L"-shaped TPAs based on their resemblance to the letter "L". Panels (d) and (h) show observations in the SH during negative and positive IMF-B_y intervals, respectively. Interestingly, these two panels appear to show the opposite chirality to their NH counterparts under the same IMF conditions, with an "L"-shaped TPA (panel d), and a "J"-shaped TPA (panel h). The detailed growth of these representative four nightside distorted TPAs and corresponding solar wind conditions are shown in the Supporting Information (Figure S1).

3.2 In-situ Duskside Magnetotail Observations during the Nightside Distorted TPA interval

All of the "J (L)"-shaped TPAs identified in our study, shown in Figure 1, originate in the nightside main auroral oval and protrude toward the dayside, indicating that nightside magnetic reconnection plays a significant role in the formation of these TPAs (see the detailed series of figures shown in Figure S1). In-situ magnetotail observations were examined during the nightside distorted TPA intervals. Figure 2 shows a summary plot of the solar wind (observed by Advanced Composition Explorer: ACE), and the magnetotail (observed by Geotail) on March 12th, 2002, when the "L"-shaped TPA was detected by IMAGE FUV-WIC. The panels from top to bottom show: the IMF-B_y and -B_z components in GSM coordinates, the solar wind dynamic pressure, the Geotail measurements of the sun-earth (GSM-X), dawn-dusk (GSM-Y) and north-south (GSM-Z) magnetic field components in the duskside magnetotail, the associated magnetic field elevation angle, and the ion flow velocity in GSM and Mean Field Coordinates (MFC), which has axes parallel and perpendicular to local magnetic field lines over the 1 hour 40 minutes time interval between 00:10 UT and 01:50 UT. During this interval, the "L"-shaped TPA intensifications were clearly identified from 00:31:34 UT to 00:58:12 UT and from 01:10:29 UT to 01:37:07 UT, which are bracketed by two gold broken lines, and labelled 'LS'. The GSM locations of Geotail when the "L"-shaped TPAs were seen are indicated below the last panel of Figure 2(a). The IMF-B_y and -B_z components were oriented roughly duskward (positive) and northward (positive) during both TPA intervals. Associated solar wind dynamic pressure showed no significant changes. The large abrupt decreases and increases twice seen in the Geotail-B_x component indicate multiple crossings (four times) of the magnetotail current sheet from the Northern to Southern, and from the Southern to Northern Hemispheres, respectively. The variations of associated B_y and B_z components were anti-correlated with that of the B_x component. Particular enhancements of the B_z component and elevation angle, seen in both LS intervals, suggest that the nightside magnetospheric configuration becomes more "dipole-like", presumably resulting from a pile-up of the magnetic flux transported from the distant magnetotail. Before the B_z enhancements, the V_x component shows earthward "bursty" enhancements, indicating the occurrence of magnetotail magnetic reconnection at the onset and the initial stage of the two "L"-shaped TPAs. Taking a look at the x-directional components of plasma flow speed parallel and perpendicular to the field lines (V_{parax}, V_{perpx}), this flow burst had a much more dominant field-aligned component (V_{parax}) than the perpendicular flow velocity (V_{perpx}). The second flow bursts seen during the second LS interval also had a strong field-aligned velocity. These earthward flow burst profiles also suggest the tailward retreat of the reconnection locations; the V_x component in the first interval had already started to decrease at the onset of the "L"-shaped TPA, and the flow burst velocity during the second "L"-shaped TPA interval was lower than that in first TPA interval (considering that there was little difference in the satellite positions between first and second TPA intervals). The V_z components at the two earthward flow bursts were negative, suggesting that the plasma in the lobe region was flowing into the reconnection region in the plasma sheet. Further energized plasma was associated with the fast plasma flows because the temperature abruptly enhanced at the time of the first flow burst, however, a significant temperature enhancement was not seen at the second fast flow event. The magnetic pressure ($B_t^2/2\mu_0$: B_t is the magnetic field intensity) was higher than the plasma pressure ($N_i kT_i$) during the two flow burst intervals, indicating that the regions where the two flow burst events occurred may be plasma sheet boundary layer (PSBL). Before the fast flow burst, Geotail was situated in the lobe region in the Northern Hemisphere, but detected the fast plasma flow just after its entry to the PSBL. This is because the plasma pressure began to gradually enhance against a slight decrease of the magnetic pressure. After the flow burst, the plasma pressure was higher than the magnetic pressure due to the migration of Geotail to the inner plasma sheet (central plasma sheet). The satellite experienced multiple crossings of the current sheet. During the second LS interval, Geotail transiently went out of the plasma sheet, and recorded a weaker second flow burst in the PSBL. After the detection of the second flow burst, the satellite returned to the inner plasma sheet. Baumjohann et al. (1988) reported that faster plasma flows in the PSBL tend to have dominant field-aligned components, that is, away from the magnetic equatorial plane, which is consistent with our interpretation in which the two flow bursts seen here occurred in the PSBL. Furthermore, these fast plasma flows seem not to be associated with a “plasma bubble” (Chen and Wolf, 1993). If “plasma bubble” structures were formed by magnetotail reconnection and resultant fast plasma flows were driven, the plasma flows should have flow velocity components dominantly perpendicular to the magnetic field lines (see figure 3 in Chen and Wolf, 1993). Chen and Wolf (1993) also pointed out that when fast bursts are caused by a “plasma bubble”, the ion temperature and the plasma pressure are gradually increased from the onset of fast flow. However, during the presented interval, the observed plasma flow bursts were predominantly field-aligned. The associated temperatures explosively increased (did not increase) in case of the first (second) flow burst, and the plasma pressure enhancements were not seen at both flow onsets. After the first flow burst, the enhancements of the plasma pressure were found because of the satellite entry to the plasma sheet.

Panels (b) and (c) of Figure 2 show zoomed-in plots of the plasma flow velocity and ground-based magnetic field perturbations measured at two ground observatories close to the TPA, for the first and second plasma flow bursts, respectively. The top two panels in each case show plasma flow velocity components in GSM coordinates and the x-directional components of plasma flow speed parallel and perpendicular to the local magnetic field, and the bottom two panels show ground magnetic field perturbations in the B_N (local magnetic north-south) and B_E (local magnetic east-west) components measured at two representative ground magnetic observatories close to the TPA. Detailed information for the ground stations is listed in Table S2 in order of geographic latitude. In the first plasma flow burst (panel b), the peaks of the V_x and V_{parax} components, and those in the ΔB_N components are seen at the same time, suggesting that the fast flows associated with magnetotail reconnection may trigger electric currents, and cause the variations of geomagnetic field. During the second flow burst interval, the geomagnetic field peaks were not seen as shown in panel (c). Therefore, at this stage of our analysis, it remains unclear whether or not electric currents which would disturb the geomagnetic field were induced by reconnection-associated fast plasma flows in this case. The summary and zoomed-in plasma velocity plots from Geotail observations of the opposite dawnside magnetotail are shown in the Supporting Information (Figure S2). Panel (d) shows the footpoints of the Geotail trajectory during the same time interval as panel (a) (1h 40m from 0:10 UT to 1:50 UT), which were calculated based on the Tsyganenko 96 empirical magnetic field model (Tsyganenko and Stern, 1996), and projected onto IMAGE FUV-WIC data on 1:20 UT. The asterisk and diamond denote the start (0:10 UT) and end (1:50 UT) times of the Geotail footpoint trajectory. During the time interval of interest, the Geotail footpoints were located in the region of 74 degrees ~ 75 degrees MLat at ~ 22 hrs MLT, and were close to the "straight bar" part of TPA in the nightside. Therefore, it is expected that the fast plasma flows associated with magnetotail magnetic reconnection, which were observed during this time interval, may play a role in the formation of the nightside distorted TPA.

3.3 Ionospheric Electric Currents Inferred from The Ground and Direct Evidence for FACs

When a shear in flow velocity exists between reconnection-associated earthward fast flows and slow magnetotail background flows is present, electric currents flowing along the geomagnetic field lines (Field-Aligned Currents: FACs) can be driven (Hasegawa and Sato, 1979; Birn and Hesse, 1991; Fairfield et al. 1999). These FACs are closely related to the auroral phenomena in the high-latitude atmosphere. In order to investigate this current system, an electric current map in the ionosphere is made based on the geomagnetic field variations beneath and in close proximity to the regions of growth of the nightside distorted ("L"-shaped) TPAs. These measurements were conducted using ground-based magnetic field observations from the SuperMAG ground observatory network (Gjerloev, 2012). Figure 3 shows the equivalent ionospheric current (EIC) distributions, projected onto the IMAGE FUV-WIC data in geomagnetic coordinates during time intervals spanning the two earthward flow bursts. The electric current maps are derived from the local magnetic north – south (B_N) and east – west (B_E) components of the geomagnetic field perturbations, which were measured at the ground magnetic observatories beneath and in close proximity to the growth regions of the nightside distorted TPA. It is well-known that these ground magnetic disturbances are generated by the horizontal components of electric currents in the ionosphere (EIC) (Glassmeier et al. 1989). The orientation and scale of FACs can also be estimated based on the EIC distributions (Glassmeier et al. 1989; Morretto et al. 1997; Motoba et al. 2003, and references therein). The geomagnetic field perturbations were taken from 50-minute-high-pass filtered B_N and B_E components. Electric current orientations were estimated by rotating these geomagnetic field fluctuation components 90 degrees clockwise (e.g., Glassmeier et al. 1989; Moretto et al. 1997). On the maps during both the first (A) and second (B) flow burst intervals, counter-clockwise current vortices were found, as indicated with magenta circular arrows. This counter-clockwise vortex-structured current suggests that FACs, oriented from the ionosphere toward the magnetotail, are caused by electron precipitation associated with reconnection-triggered plasma flow bursts, which were observed by Geotail. This result also suggests that the energized plasma (electrons) were conveyed by the magnetotail fast flows from the magnetotail to the ionosphere. The vortex spatial scale appears to be different between first and second interval. In panels (A), a "large-scale" vortex-like current structure is discerned by the electric current vectors measured at most observatories, which are mainly located in the dusk sector (westside) of the nightside distorted TPA, while "small-scale" current vortices with a similar rotational sense are indicated on the nightside part of the TPA during the second interval (panels B). Neither vortex current structure showed any poleward (high-latitude) migration as the "L"-shaped TPA grew to the dayside.

The vortex-like ionospheric current structures, deduced from the geomagnetic field fluctuations, indicate that upward (from the ionosphere toward the magnetotail) FACs play an essential role in the formation of nightside distorted TPAs. To obtain clearer evidence for the presence of FACs associated with the TPAs, we investigated whether or not the DMSP (Defense Meteorological Satellite Program) satellites crossed the TPAs, and could measure the associated magnetic field to extract the current density along the magnetic field lines (FACs). From our 9 TPA events, we found that the DMSP-F13, -F14 and -F16 satellites crossed the dayside straightforward bar-shaped part of the “L”-shaped TPA, as seen on 28th October 2003.

Figure 4 shows the temporal variations of the current density parallel to the magnetic field lines (J_{para}) derived by the DMSP magnetic field data, which are plotted against universal time (UT), and the DMSP tracking information, such as MLat, magnetic longitude (MLON) and MLT. The current density can be computed by applying Ampère’s law to the magnetic field perturbations, measured just before and after the DMSP-F13 (panel a), -F14 (panel b) and -F16 (panel c) crossings of the TPA. More detailed theory and techniques to derive the current density from the magnetic field data are described by Wang et al. (2005) and Lühr et al. (2016). During the DMSP crossing interval of each TPA (in each case less than1 minute), bracketed by two magenta broken lines, negative J_{para} values were found. This indicates that upward FACs were flowing out of the TPA (Wang et al., 2005). The geomagnetic field measurements on ground showed large- and small-scale counter-clockwise vortex-like current structures beneath and in close proximity to the TPA, and negative J_{para} bays were found during the DMSP TPA crossings. These results indicate that upward FACs are a dominant source of the nightside distorted TPAs.

3.4 Retreat of Reconnection Points

The electric current vortices suggest that FACs may be essential to formation of the nightside distorted TPA. Here, we consider the “growth” of the TPA. According to the conventional model to explain the TPA formation based on nightside reconnection (Milan et al. 2005), which does not take into account the influence of FACs in the TPA formation, the reconnection points should retreat tailward as the TPA grows to the dayside. A summary plot of the Geotail observations shown in Figure 2 has already suggested the tailward retreat of the reconnection point. To further support this scenario, we examine the geomagnetic field variations associated with the nightside distorted TPAs using ground-based observations. Figure 5(A) shows geomagnetic field observations at several ground magnetic observatories corresponding to the locations beneath or in close proximity to the regions of growth of a nightside distorted TPA (“L”-shaped TPA observed on 12th March 2002). All magnetic field data for the ground observatories were taken from the SuperMAG network (Gjerloev, 2012). Several magenta points labelled with numbers in the IMAGE FUV-WIC plots in panel (b) correspond to similarly labelled locations in geographical map (panel c). Panel (a) in figure 5(A) shows a stack plot of fluctuations in the local (magnetic) north-south geomagnetic field component (ΔB_N) at these observatories, which are shown by blue. The magnetic fluctuations are obtained by the subtraction of the average magnetic field over the time interval of interest from the raw magnetic field values. The fluctuation component at each station is plotted upon their averages as indicated by horizontal grey broken lines, and its peak during the "L"-shaped TPA intensification intervals, bracketed by two gold broken lines, is marked by magenta open circle. The plots are sorted in decreasing order of latitude. The magnetic field fluctuation component at the time of panel (b) (00:39:45 UT) is indicated by a vertical cyan solid line in the panel (a). The color code of the IMAGE FUV-WIC data in panel (b) is assigned according to ADU.

Figure 5(B) shows a scatter plot of the time-delay of the fluctuation peaks in the local (magnetic) north-south magnetic field component (ΔB_N) from the onset times of 5 nightside distorted TPAs at several ground magnetic observatories from geographical low- to high-latitudes. The detailed geomagnetic field plots and information on the ground magnetic observatories in the other four TPA events, except for the 12th March 2002 event, are shown in the Supporting Information (Figure S3). All peaks seen in the magnetic field fluctuation components were positive, implying enhancements of FACs flowing out of the ionosphere, that is, downflowing of electrons from the magnetotail. For three of the TPAs (2000/09/22, 2001/12/31 and 2002/03/02), the magnetic peaks are clearly seen at later times for observatories with higher latitude, suggesting that the reconnection points (the source regions of the energetic electrons) were retreating further down-magnetotail, associated with the growth of the TPA to the dayside. This result supports not only the tail reconnection occurrence but also the retreat of the reconnection points. The average velocity of the reconnection point retreat can roughly be estimated based on the slope of a line of geographical latitude versus the time delay between the magnetic peaks and the TPA onsets. We adopted a value of 1 degree = 110.95 km to convert a unit of geographic latitude (degree) to equatorial distance (km). The estimated reconnection point retreat velocity is summarized in the table in the top-right of the figure. The three TPAs mentioned above, with very apparent reconnection point retreats, had reconnection point retreat velocities within a range between about 1.2 km/s and 3.0 km/s. The others (2000/11/05 and 2002/03/12) showed a much faster retreat speed (7.3 km/s and 12.3 km/s) because their magnetic field peaks appeared with much lower time lags, irrespective of the latitudes of the observatory locations.

3.5 Persistence of Magnetotail Reconnection During the Northward IMF Interval

We discuss the plasma flows and their patterns in the polar cap region measured by Super Dual Auroral Radar Network High Frequency (SuperDARN HF) radars (Greenwald et al. 1995; Chisham et al. 2007) during the nightside distorted TPA intervals, in order to obtain evidence for the persistence of magnetotail magnetic reconnection even under northward IMF conditions. The SuperDARN radars, which are located in the high-latitude regions in both Northern and Southern Hemispheres, provide line-of-sight ionospheric plasma flow velocity over much of the polar and auroral regions. These measurements, particularly obtained from nine SuperDARN radars in the Northern Hemisphere, have been used to produce high-latitude convection maps based on the "Map Potential" technique (Ruohoniemi and Baker, 1998). The line-of-sight velocity vectors are projected onto geomagnetic grids, and fitted to electrostatic potential solutions, which are described by a sixth order spherical harmonic expansion. Complementary flow data from a statistical model characterised by upstream IMF conditions (Ruohoniemi and Greenwald, 1996) is used to constrain the construction of the large-scale flow pattern in regions where the radars provide no measurements (Ruohoniemi and Baker, 1998).

Figure 6 presents 6 selected 2 minutes integrations of the northern hemispheric plasma flow streamlines and drift velocity vectors during the interval of a nightside distorted TPA ("J"-shaped TPA) observed on 31st December 2001. We overlay these flow velocity profiles onto the corresponding IMAGE FUV-WIC auroral imager data. Black regions indicate higher auroral luminosity, and the IMAGE observation time is shown at the top in each panel. The left, bottom and right sides in each panel correspond to 18h, 24h, and 6h in magnetic local time, respectively. The dotted semicircles indicate the magnetic latitude (MLat) range between 60 degrees and 80 degrees. During the growth of the "J"-shaped TPA, westward plasma flows, ranging between 0.35 km/s and 0.85 km/s, were locally (although non-continuously) observed at the poleward edge of the midnight-sector main auroral oval, highlighted by magenta ovals. These flows were originally oriented toward the equator, but rotated toward the west at the poleward edge of the main auroral oval. They are highly suggestive of magnetic reconnection in the magnetotail, identified as "Tail Reconnection during IMF Northward and Non-substorm Intervals (TRINNIs)" (Grocott et al. 2003, 2004) under dawnward IMF-B_y conditions (see the IMF condition shown in Figure S1c) (Milan et al. 2005; Grocott et al. 2003, 2004). Therefore, at least, nightside reconnection was ongoing during the growth of the "J"-shaped TPA even under the northward IMF conditions, and should play a significant role in the nightside distorted TPA formation.

4. Discussion

4.1 A Possible Formation Scenario of the Nightside Distorted TPA

The conventional TPA formation model proposed by Milan et al. (2005) is based on the magnetospheric convection of closed magnetic fluxes formed by magnetotail reconnection. The ground-based observations revealed that the reconnection points retreated tailward with the poleward growth of the TPAs. Furthermore, the SuperDARN HF radar detected TRINNIs, which are remote-sensing evidence for persistent magnetotail reconnection under the northward IMF conditions, being consistent with the framework of the conventional TPA formation model (Milan et al. 2005). However, our observations show that FACs can be generated by a plasma flow shear between the fast plasma flows triggered by nightside magnetic reconnection and background magnetospheric slow plasma flows, and appear to play an essential role in the formation of nightside distorted TPAs. In Figure 3, counter-clockwise vortex-like ionospheric current structures are detected by ground-based magnetic field observations beneath and in close proximity to the growth regions of the nightside distorted TPAs during the plasma flow bursts seen in the magnetotail. The current density component along magnetic field lines derived by the magnetic field perturbations during the DMSP satellite crossings of the TPA show significant negative bays in Figure 4. These observations suggest the presence of upward FACs associated with nightside distorted TPAs.

Taking into account these observations, we construct a model to illustrate nightside distorted TPA (in particular, “L”-shaped TPA) formation. Figure 7 displays a schematic diagram of the possible formation process of an “L”-shaped TPA under positive (duskward) IMF-B_y conditions. The main “bar-like” emissions of the nightside distorted TPAs are located on the dusk side under positive IMF-B_y conditions as seen in Figure 1. The location of the “L”- (“J”)-shaped TPAs strongly depends on the IMF-B_y sign; the relation between the location of the main TPA part and the IMF-B_y polarity is the same as that for the “regular” TPA (Comnock et al. 2002; Kullen et al. 2002) (see the plots of the OMNI and Geotail-measured solar wind data in Figure S1). This model is depicted in terms of the configuration changes of magnetic field lines due to magnetospheric convection, FACs, reconnection-associated plasma flows, and the reconnection point retreat. The closed field lines formed by nightside reconnection are illustrated by thick blue solid curves, and the orange curves indicate the electric currents induced by the plasma flow shear between the background slow plasma flows and fast flows originating from magnetotail magnetic reconnection (blue arrows). FACs flowing out of the ionosphere toward the magnetotail constitute the “source” of the nightside distorted TPAs, being consistent with large- and small-scale electric current vortices beneath and in close proximity to the growth regions of the nightside distorted TPAs, and significant negative bays of the current density component along the magnetic field lines (J_{para}) across the TPA. Magnetotail reconnection continues at the point denoted by red dots until the TPA completely forms, and associated closed field lines convect earthward. The reconnection location retreats further tailward from T_0 to T_3, which are highlighted by the thick red arrows and the pink-shaded area, as the tip of the TPA approaches the dayside. This is because higher latitude field lines within the TPA have their nightside (equatorial crossing) positions further down-tail.

As the reconnection points retreat tailward, the TPA-associated closed flux tubes are contemporaneously twisted clockwise (counter-clockwise), depending on the dawnward (duskward) IMF-B_y component. Meanwhile, the nightside plasma sheet undergoes an oppositely-oriented deformation (Tsyganenko et al. 2015; Tsyganenko and Fairfield, 2004), indicated by inclined red bar in Figure 7. The closed flux tube twisting is caused by the IMF-B_y penetration, which produces “asymmetry” for the magnetic fields in the Northern and Southern Hemisphere, exerting “torque rotation” due to the electromagnetic force (Gosling et al. 1990; Cowley, 1981, 1994). This results in the “L”- and “J”-shaped TPAs, corresponding to the ionospheric footpoints of these field lines in the Northern and Southern Hemispheres.

Before and during all nightside distorted TPAs examined in this study (listed in Table S1), the IMF-B_z had been dominantly northward, however magnetotail reconnection appears to occur and, at least, persist during the TPA interval. This result is supported by significant enhancements in geomagnetic activity even under strong and persistent northward IMF-B_z conditions (Shi et al. 2012), and indicates that solar wind energy can enter the magnetosphere during the northward IMF intervals.

Zhu et al. (1997) suggests that the FACs associated with polar cap arcs (TPAs) indicate the presence of upward and downward current pairs. Chen and Wolf (1993) proposed a model of closure of upward and downward FACs in the dawn and dusk sectors, which are linked with the inertial currents in the magnetotail and the currents perpendicular to the magnetic field line in the ionosphere. In this model, it is considered that the magnetotail-ionosphere FACs were generated by the reconnection fast flows driven by a "plasma bubble". However, in our model, TPA-associated magnetic field lines are closed by magnetotail reconnection, and FACs, which are the source of the TPA, may be caused by the flow shear due to the reconnection-associated fast plasma flows. This model simply explains that the nightside distorted TPA is comprised of only closed field lines that have been recently generated by nightside magnetic reconnection, and does not include the fate of other regions of closed fluxes which do not significantly contribute to the formation of the nightside distorted TPA.

Because the contribution of a "plasma bubble" for the observed fast flows seems to be small or insignificant, as shown in Figure 2, the bubble-associated current closure scenario is not well supported. In this study, sufficient data is unavailable to make an ionospheric current map that would reveal the global FAC profile in the Northern (Southern) Hemisphere. A series of studies based on a global MHD simulation (e.g., Tanaka et al. 2004; Watanabe et al. 2013) showed and discussed a large-scale profile of FAC distributions associated with TPA formation. Upward (downward) FACs can be developed in the sector opposite to the downward (upward) FACs, so that closed current systems are formed, but the development processes during the TPA growth are complicated. In particular, Watanabe et al. (2013) showed that multiple current closures, consisting of multiple upward and downward FACs, can be formed during the TPA growth. At this stage, the global FAC structure associated with the nightside distorted TPAs is not yet revealed with in-situ geomagnetic field measurements. This is a problem to be clarified in the future. In Figure S4, the SuperDARN radar data during this "L"-shaped TPA detected counter-clockwise ionospheric plasma flows in the dawnside in the Northern Hemisphere. These plasma flow patterns (vortex-like plasma flows) may indicate that the clockwise ionospheric currents, that is, downward FACs, can be generated (e.g., Moretto et al. 1997; Motoba et al. 2003). However, in order to reveal the complete current system associated with the nightside distorted TPAs with greater certainty, a more extensive set of geomagnetic field observations is required.

4.2 Scale of Electric Current Vortex Associated with Nightside Distorted TPA

The electric current vortices provide indicative evidence of FACs flowing out of the ionosphere to the magnetotail. However, their scales were found to be different between two nightside distorted TPA intervals: a large-scale vortex was seen during the first interval, whereas during the second "L"-shaped TPA interval, local small-scale vortices were found at the observatories near the TPA. Since these FACs were induced by the plasma flow shear, the velocity of the plasma flows associated with magnetotail reconnection would be a key physical parameter to determine the current vortex scale on the ground. Therefore, the current vortex scale might be roughly proportional to the plasma flow speed. The electric current vortex scale should become smaller, if the energy of plasma (electrons) released by magnetic reconnection in the magnetotail was dissipated upon the ionosphere (Tanskanen et al. 2002).

4.3 Formation of the Distortions at TPA Nightside Ends

After the onset of nightside reconnection, the reconnection locations retreated tailward as the tips of the TPAs (in Northern and Southern Hemispheres) approach the dayside, and apparently become "stagnant points", which are unaffected by magnetospheric convection. Furthermore, the closed flux tubes within the nightside distorted TPAs, which are generated by persistent nightside reconnection even under northward IMF conditions, are twisted, associated with the magnetotail deformation. During the growth of nightside distorted TPA under the significant IMF-B_y conditions as the reconnection site moves further tailward, the tail deformation becomes larger and associated field lines are also twisted more strongly (Tsyganenko et al. 2015; Tsyganenko and Fairfield, 2004). Significantly, this twisting of field lines, caused by the IMF-B_y penetration (Gosling et al. 1990; Cowley, 1981, 1994), gives opposite chirality to the "J"- and "L"-shaped TPAs seen in the Northern and Southern Hemispheres, even though magnetotail magnetic reconnections occur at the "same" locations in the Northern and Southern Hemispheres (see Figure 7). In a previous study (Milan et al. 2005), it was considered that the nightside magnetospheric deformation and field line twisting are only important in determining the TPA growth point in the nightside main auroral oval. Our scenario, however, emphasizes that they play an important role in determining not only the TPA morphology but also how the plasma (electrons) released by magnetotail reconnection are supplied to the ionosphere.

5. Conclusions

In this study, we have demonstrated that investigations of TPA morphology are important in assessing how the energy stored in the deformed magnetotail is released and supplied to the high-latitude atmosphere or ionosphere. In particular, we have shown that the nightside distorted TPA is a good remote-sensing diagnostic tool for monitoring global magnetospheric effects. The fundamental characteristics and the formation scenario of nightside distorted TPAs obtained through this study have clear potential for application to other planets. Namely, this study contributes to understanding the roles of the IMF and solar wind plasma in auroral processes, which can also occur at other planets of solar system. Hereafter, more detailed observations of the solar wind-magnetosphere-ionosphere coupling are required to better understand the process of nightside distorted TPA formation.

Acknowledgments

This work is supported by grants of the National Natural Science Foundation of China (NSFC 41961130382, 41974189, and 41404131). B.H. is supported by the Belgian National Fund for Scientific Research (FNRS). A.W.D is supported by NSFC grant (41774172). A.G. is supported by STFC grant (ST/R000816/1) and NERC grants (NE/P001556/1 and NE/T000937/1). M.N. thanks Anthony T. Y. Lui for constructive and insightful discussion on our obtained results, and for modeling of the nightside distorted TPAs, and Chen-Yao Han for helping to draw Figure 7. Also, he thanks Yukinaga Miyashita for helping the MFC/FAC coordinate transformation of the Geotail plasma data, and the calculations of the Geotail footpoints on ionosphere. We thank the PIs of the SuperDARN radars for provision of the ionosphere flow data. SuperDARN is funded by the research agencies of Australia, China, Canada, France, Italy, Japan, South Africa, the U. K. and the U. S. For the ground magnetometer data we gratefully acknowledge: Intermagnet; USGS, Jeffrey J. Love; CARISMA, PI Ian Mann; CANMOS, Geomagnetism Unit of the Geological Survey of Canada; The S-RAMP Database, PI K. Yumoto and Dr. K. Shiokawa; The SPIDR database; AARI, PI Oleg Troshichev; The MACCS program, PI M. Engebretson; GIMA; MEASURE, UCLA IGPP and Florida Institute of Technology; SAMBA, PI Eftyhia Zesta; 210 Chain, PI K. Yumoto; SAMNET, PI Farideh Honary; The IMAGE magnetometer network, PI L. Juusola; AUTUMN, PI Martin Connors; DTU Space, PI Anna Willer; South Pole and McMurdo Magnetometer, PI's Louis J. Lanzarotti and Alan T. Weatherwax; ICESTAR; RAPIDMAG; British Artarctic Survey; McMac, PI Dr. Peter Chi; BGS, PI Dr. Susan Macmillan; Pushkov Institute of Terrestrial Magnetism, Ionosphere and Radio Wave Propagation (IZMIRAN); GFZ, PI Dr. Juergen Matzka; MFGI, PI B. Heilig; IGFPAS, PI J. Reda; University of L'Aquila, PI M. Vellante; BCMT, V. Lesur and A. Chambodut; Data obtained in cooperation with Geoscience Australia, PI Marina Costelloe; AALPIP, co-PIs Bob Clauer and Michael Hartinger; SuperMAG, PI Jesper W. Gjerloev; Sodankylä Geophysical Observatory, PI Tero Raita; Polar Geophysical Institute, Alexander Yahnin and Yarolav Sakharov; Geological Survey of Sweden, Gerhard Schwartz; Swedish Institute of Space Physics, Mastoshi Yamauchi; UiT the Arctic University of Norway, Magnar G. Johnsen; Finish Meteorological Institute, PI Kirsti Kauristie.

Data Availability

IMAGE FUV-WIC data can be obtained by contacting the corresponding authors (M.N. and B.H.) and can also be accessed from http://image.gsfc.nasa.gov. SuperDARN data is freely provided for scientific research purposes and can be obtained from the SuperDARN data mirror (http://bslsuperdarnc.nerc-bas.ac.uk:8093/docs/) or by contacting any of the SuperDARN PI research groups (http://www.superdarn.ac.uk). All SuperDARN radar data are processed by the software of fitacf v1.2 and make_grid v1.14.er which are part of the Radar Software Toolkit (RST v4.2 https://zenodo.org/record/1403226#.Xy0u7y3MxTY). OMNI (ACE) IMF and solar wind plasma were obtained from Coordinated Data Analysis Web (https://cdaweb.sci.gsfc.nasa.gov/index.html/), provided by NASA Goddard Flight Space Flight Center (GSFCs) Space Physics Data Facility. The Geotail MGF and CPI data can be obtained from Data ARchives and Transmission System (DARTS), provided by the Center for Science-satellite Operation and Data Archive (C-SODA) at ISAS/JAXA (http://darts.isas.jaxa.jp/about.html.en). The ground magnetic field data used in this paper can be downloaded from the SuperMAG website (http://supermag.jhuapl.edu/). We also thank the World Data Centre for Geomagnetism, Kyoto University for accessing the data of *AU* and *AL* indices from http://wdc.kugi.kyoto-u.ac.jp/index.html. The triaxial fluxgate magnetometer data of DMSP (Defense Meteorological Satellite Program) with 1 second temporal resolution are accessible from the website of the database of the Coupling, Energetics and Dynamics of Atmospheric Regions (CEDAR)/Madrigal (http://cedar.openmadrigal.org/list/ and https://dmsp.bc.edu/html2/dmspssm.html).

References

Angelopoulos, V., Baumjohann, W., Kennel, C. F., Coroniti, F. V., Kivelson, M. G., Pellat, R., et al. (1992), Bursty bulk flows in the inner central plasma sheet. Journal of Geophysical Research: Space Physics, 97, 4027 – 4039.

Angelopoulos, V., Kennel, C. F., Coroniti, F. V., Pellat, R., Kivelson, M. G., Walker, R. J., Russell, C. T., Baumjohann, W., Feldman, W. C., and Gosling, J. T. (1994), Statistical characteristics of bursty bulk flow events, Journal of Geophysical Research: Space Physics, 99(A11), 21257–21280, doi:10.1029/94JA01263.

Angelopoulos, V., et al. (1996), Multipoint analysis of a bursty bulk flow event on April 11, 1985, Journal of Geophysical Research: Space Physics, 101(A3), 4967– 4989, doi:10.1029/95JA02722.

Angelopoulos, V., Runov, A., Zhou, X.-Z., Turner, D. L., Kiehas, S. A., Li, S.-S., Shinohara, I. (2013). Electromagnetic energy conversion at reconnection fronts. Science, 341(6153), 1478 – 1482. https://doi.org/10.1126/science.1236992.

Baumjohann, W., Paschmann, G., and Cattell, C. A. (1989), Average plasma properties in the central plasma sheet, Journal of Geophysical Research: Space Physics, 94(A6), 6597– 6606, doi:10.1029/JA094iA06p06597.

Baumjohann, W., Paschmann, G., and Lühr, H. (1990), Characteristics of high−speed ion flows in the plasma sheet, Journal of Geophysical Research: Space Physics, 95(A4), 3801– 3809, doi:10.1029/JA095iA04p03801.

Baumjohann, W., Paschmann, G., Sckopke, N., Cattell, C. A., and Carlson, C. W. (1988), Average ion moments in the plasma sheet boundary layer, Journal of Geophysical Research: Space Physics, 93(A10), 11507 – 11520, doi:10.1029/JA093iA10p11507.

Birn, J., and Hesse, M., The substorm current wedge and field-aligned currents in MHD simulations of magnetotail reconnection, J. Geophys. Res.: Space physics, 96, A2, 1611 – 1618, (1991).

Black, D. I., Cosmic ray effects and faunal extinctions at geomagnetic field reversals, Earth Planet. Sci. Lett. 3, 225–236, (1967).

Chen, C. X., and Wolf, R. A. (1993), Interpretation of high‐speed flows in the plasma sheet, Journal of Geophysical Research: Space Physics, 98(A12), 21409 – 21419, doi:10.1029/93JA02080.

Chisham, G., Lester, M., Milan, S. E., Freeman, M. P., Bristow, W. A., Grocott, A., McWilliams, K. A., Ruohoniemi, J. M., Yeoman, T. K., Dyson, P. L., Greenwald, R. A., Kikuchi, T., Pinnock, M., Rash, J. P. S., Sato, N., Sofko, G. J., Villain, J.-P., and Walker, A. D. M., A decade of the Super Dual Auroral Radar Network (SuperDARN): Scientific achievements, new techniques and future directions. Surveys in Geophysics, 28(1), 33 – 109, (2007).

Cowley, S. W. H., Magnetospheric asymmetries associated with the y-component of the IMF, Planet. Space Sci., 29, 79 – 96, (1981).

Cowley, S. W. H., Earth's plasma environment: magnetic reconnection and its effect on magnetospheric fields and flows, Philosophical Transaction: Physical Sciences and Engineering, 349, 1690, The Solar-System: A Review of Results from Space Mission (Nov. 15), 237 – 247, (1994).

Cumnock, J. A., Sharber, J. R., Heelis, R. A., Blomberg, L. G., Germany, G. A., Spann, J. F., and Coley, W. R., Interplanetary magnetic field control of theta aurora development, J. Geophys. Res.: Space physics, 107(A7), 1108, (2002).

Fairfield, D. H., Mukai, T., Brittnacher, M., Reeves, G. D., Kokubun, S., Parks, G. K., Nagai, T., Matsumoto, H., Hashimoto, K., Gurnett, D. A., and Yamamoto, T., Earthward flow bursts in the inner magnetotail and their relation to auroral brightenings, AKR intensifications, geosynchronous particle injections and magnetic activity, J. Geophys. Res.: Space physics, 104, A1, 355 – 370, (1999).

Fear, R. C. and Milan, S. E., The IMF dependence of the local time of transpolar arcs: Implications for formation mechanism, J. Geophys. Res.: Space physics, 117(A03213), (2012a).

Fear, R. C. and Milan, S. E. Ionospheric flows relating to transpolar arc formation, J. Geophys. Res.: Space physics, 117, A09230, (2012b).

Frank, L. A., Craven, J. D., Burch, J. L., and Winningham, J. D., Polar views of the Earth's aurora with Dynamics Explorer, Geophys. Res. Lett., 9(9), 1001 – 1004, (1982).

Gjerloev, J. W., The SuperMAG data processing technique, J. Geophys. Res.: Space physics, 117, A09213, (2012).

Glassmeier, K. -H., Hönisch, M., and Untiedt, J., Ground-based and spacecraft observations of traveling magnetospheric convection twin vortices, Journal of Geophyocal Research: Space physics, 94, 2520–2528, (1989).

Glassmeier, K. -H., Richter, O., Vogt, J., Möbus, P., and Schwalb, A., The Sun, geomagnetic polarity transitions, and possible biospheric effects: review and illustrating model. Int. J. Astrobiol., 8, 147–159, (2009).

Glassmeier, K. -H., and Vogt, J., Magnetic polarity transitions and biospheric effects, Space Sci. Rev., 155, 1-4, 387 – 410, (2010).

Gosling, J. T., Thomsen, M. F., Bame, S. J., Elphic, R. C., and Russell, C. T., Plasma flow reversals at the dayside magnetopause and the origin of asymmetric polar cap convection, J. Geophys. Res.: Space physics, 95(A6), 8073 – 8084, (1990).

Greenwald, R. A., Baker, K. B., Dudeney, J. R., Pinnock, M., Jones, T. B., Thomas, E. C., Villain, J. -P., Cerisier, J. -C., Senior, C., Hanuise, C., Hunsucker, R. D., Sofko, G., Koehler, J., Nielsen, E., Pellinen, R., Walker, A. D. M., Sato, N., and Yamagishi, H., DARN/SuperDARN: A global view of high latitude convection, Space Sci. Rev., 71(1-4), 761 – 796, (1995).

Grocott, A., Cowley, S. W. H., and Sigwarth, J. B., Ionospheric flow during extended intervals of northward but B_Y-dominated IMF, Ann. Geophys., 21(2), 509 – 538, (2003).

Grocott, A., Badman, S. V., Cowley, S. W. H., Yeoman, T. K., and Cripps, P. J., The influence of IMF B_Y on the nature of the nightside high-latitude ionospheric flow during intervals of positive IMF B_Z, Ann. Geophys., 22(5), 1755 – 1764, (2004).

Grocott, A., Yeoman, T. K., Milan, S. E., Amm. O., Frey, H. U., Juusola, L. et al., Multi-scale observations of magnetotail flux transport during IMF-northward non-substorm intervals. Ann. Geophys., 25, 1709-1720. doi:10.5194/angeo-25-1709-2007, (2007).

Hasegawa, A., and Sato, T., Generation of Field Aligned Current During Substorm. In: Akasofu SI. (eds) Dynamics of the Magnetosphere. Astrophysics and Space Science Library (A Series of Books on the Recent Developments of Space Science and of General Geophysics and

Astrophysics Published in Connection with the Journal Space Science Reviews), 78. Springer, Dordrecht, (1979).

Heppner, J. P., and Maynard, N. C., Empirical high-latitude electric field models, J. Geophys. Res.: Space physics, 92, 4467 – 4489, (1987).

Kaymaz, Z., Siscoe, G., Luhmann, J. G., Fedder, J. A., and Lyon, J. G., Interplanetary magnetic field control of magnetotail field: IMP 8 data and MHD model compared, J. Geophys. Res.: Space physics, 100, A9, 17,163 – 17,172, (1995).

Kullen, A., Brittnacher, M., Cumnock, J. A., and Blomberg, L. G., Solar wind dependence of the occurrence and motion of polar auroral arcs: A statistical study, J. Geophys. Res.: Space physics, 107(A11), 1362, (2002).

Kullen, A., Fear, R. C., Milan, S. E., Carter, J. A., and Karlsson, T., The statistical difference between bending arcs and regular polar arcs, J. Geophys. Res.: Space physics, 120, (2015).

Lühr, H., Huang, T., Wing, S., Kervalishvili, G., Rauberg, J., and Korth, H. (2016), Filamentary field-aligned currents at the polar cap region during northward interplanetary magnetic field derived with the Swarm constellation, Ann. Geophys., 34, 901 – 915, https://doi.org/10.5194/angeo-34-901-2016.

Milan, S. E., Hubert, B., and Grocott, A., Formation and motion of a transpolar arc in response to dayside and nightside reconnection, J. Geophys. Res.: Space physics, 110, A01212, (2005).

Mende, S. B., Heetderks, H., Frey, H. U., Lampton, M., Geller, S. P., Habraken, S., Renotte, E., Jamar, C., Rochus, P., Spann, J., Fuselier, S. A., Gerard, J. -C., Gladstone, R., Murphree, S., and Cogger, L., Far ultraviolet imaging from the IMAGE spacecraft: 1. System design, Space Sci. Rev., 91, 243 – 270, (2000).

Mende, S. B., Heetderks, H., Frey, H. U., Lampton, M., Geller, S. P., Abiad, R., Siegmund, O. H. W., Tremsin, A. S., Spann, J., Dougani, H., Fuselier, S. A., Magoncelli, A. L., Bumala, M. B., Murphree, S., and Trondsen, T., Far ultraviolet imaging from the IMAGE spacecraft: 2. Wideband FUV imaging, Space Sci. Rev., 91, 271 – 285, (2000).

Mende, S. B., Heetderks, H., Frey, H. U., Stock, J. M., Lampton, M., Geller, S. P., Abiad, R., Siegmund, O. H. W., Habraken, S., Renotte, E., Jamar, C., Rochus, P., Gerard, J. -C., Sigler, R., and Lauche, H., Far ultraviolet imaging from the IMAGE spacecraft: 3. Spectral imaging of

Lyman-α and OI 135.6 nm, Space Sci. Rev., 91, 287 – 318, (2000).

Motoba, T., Kikuchi, T., Okuzawa, T., and Yumoto, K. (2003), Dynamical response of the magnetosphere-ionosphere system to a solar wind dynamic pressure oscillation, Journal of Geophysical Research: Space Physics, 108(A5), 1206, doi:10.1029/2002JA009696.

Moretto, T., Friis-Christensen, E., Lühr, H., and Zesta, E. (1997), Global perspective of ionospheric traveling convection vortices: Case studies of two Geospace Environmental Modeling events, Journal of Geophysical Research: Space Physics, 102(A6), 11597– 11610, doi:10.1029/97JA00324.

Nagai, T., Shinohara, I., Fujimoto, M., Hoshino, M., Saito, Y., Machida, S., and Mukai, T. (2001), Geotail observations of the Hall current system: Evidence of magnetic reconnection in the magnetotail, Journal of Geophysical Research: Space Physics, 106(A11), 25929 – 25949, doi:10.1029/2001JA900038.

Nishida, A., Mukai, T., Yamamoto, T., Saito, Y., Kokubun, S., and Maezawa, K., GEOTAIL observation of magnetospheric convection in the distant tail at 200 R_E in quiet times, J. Geophys. Res.: Space physics, 100, A12, 23,663 – 23,675, (1995).

Nishida, A., Mukai, T., Yamamoto, T., Kokubun, S., and Maezawa, K., A unified model of the magnetotail convection in geomagnetically quiet and active times J. Geophys. Res.: Space physics, 103, A3, 4409 – 4418, (1998).

Nowada, M., Fear, R. C., Grocott, A., Shi, Q. -Q., Yang, J., Zong, Q. -G., Wei, Y., Fu, S. -Y., Pu, Z. -Y., Mailyan, B., and Zhang, H., Subsidence of ionospheric flows triggered by magnetotail magnetic reconnection during transpolar arc brightening, J. Geophys. Res.: Space physics, 123, (2018).

Petrukovich, A. A., Sergeev, V. A., Zelenyi, L. M., Mukai, T., Yamamoto, T., et al. (1998). Two spacecraft observations of a reconnection pulse during an auroral breakup. Journal of Geophysical Research, 103(A1), 47–59. https://doi.org/10.1029/97JA02296.

Pitkänen, T., Hamrin, M., Norqvist, P., Karlsson, T., and Nilsson, H., IMF dependence of the azimuthal direction of earthward magnetotail fast flows, Geophys. Res. Lett., 40, 5598, (2013).

Pitkänen, T., Hamrin, M., Norqvist, P., Karlsson, T., Nilsson, H., Kullen, A., Imber, S. M., and Milan, S. E., Azimuthal velocity shear within an earthward fast flow: Further evidence for magnetotail untwisting, Ann. Geophys., 33, 245, (2015).

Pitkänen, T., Hamrin, M., Karlsson, T., Nilsson, H., and Kullen, A., On IMF By-induced dawn-dusk asymmetries in earthward convective fast flows. In S. Haaland, A. Runov, & C. Forsyth (Eds.), Dawn-dusk asymmetries in planetary plasma environments, Geophyscial Monograph Series, 95–106, Hoboken, NJ: John Wiley, (2017).

Ruohoniemi, J. M., and Baker, K. B., Large-scale imaging of high-latitude convection with Super Dual Auroral Radar Network HF radar observations, J. Geophys. Res.: Space physics, 103(A9), 20797 – 20811, (1998).

Ruohoniemi, J. M., and Greenwald, R. A., Statistical patterns of high-latitude convection obtained from Goose Bay HF radar observations, J. Geophys. Res.: Space physics, 101(A10), 21743 – 21763, (1996).

Shi, Q. -Q., Zong, Q. -G., Fu, S. -Y., Dunlop, M. W., Pu, Z. -Y., Parks, G. K., Wei, Y., Li, W. -H., Zhang, H., Nowada, M., Wang, Y. B., Sun, W. -J., Xiao, T., Rème, H., Carr, C., Fazakerley, A. N., and Lucek, E., Solar wind entry into the high-latitude terrestrial magnetosphere during geomagnetically quiet times. Nat. Commun., 4, 1466, (2013).

Shi, X. -F., Zong, Q. -G., and Wang, Y. -F., Comparison between the ring current energy injection and decay under southward and northward IMF B_z conditions during geomagnetic storms, Sci. China Tech, Sci., 55, 10, 2769 – 2777, (2012).

Tanaka, T., T. Obara, and M. Kunitake (2004), Formation of the theta aurora by a transient convection during northward interplanetary magnetic field, Journal of Geophysical Research: Space Physics, 109, A09201, doi:10.1029/2003JA010271.

Tanskanen, E., Pulkkinen, T. I., Koskinen, H. E. J., and Slavin, J.A., Substorm energy budget during low and high solar activity: 1997 and 1999 compared, J. Geophys. Res.: Space Physics, 107(A6), 1086, (2002).

Tenfjord, P., Østgaard, N., Snekvik, K., Laundal, K. M., Reistad, J. P., Haaland, S., and Milan, S. E., How the IMF B_y induces a B_y component in the closed magnetosphere and how it leads to asymmetric currents and convection patterns in the two hemispheres, J. Geophys. Res.: Space Physics, 120, 9368 – 9384, (2015).

Tenfjord, P., Østgaard, N., Haaland, S., Snekvik, K., Laundal, K. M., Reistad, J. P., Strangeway, R., Milan, S. E., Hesse, M., and Ohma, A., How the IMF B_y induces a local By component during northward IMF B_z and characteristic timescales, J. Geophys. Res.: Space physics, 123, (2018).

Tsyganenko, N. A., and Stern, D. P. (1996), Modeling the Global Magnetic Field of the Large-Scale Birkeland Current Systems, J. Geophys.Res.: Space Physics, 101, 27187 - 27198.

Tsyganenko, N. A., Andreeva, V. A., and Gordeev, E. I. (2015), Internally and externally induced deformations of the magnetospheric equatorial current as inferred from spacecraft data, Ann. Geophys., 33, 1 – 11.

Tsyganenko, N. A., and Fairfield, D. H. (2004), Global shape of the magnetotail current sheet as derived from Geotail and Polar data, J. Geophys. Res.: Space physics, 109(A03218).

Tsyganenko, N. A., and Sitnov, M. I. (2005), Modeling the dynamics of the inner magnetosphere during strong geomagnetic storms, J. Geophys. Res.: Space physics, 110 (A3), A03208.

Wang, C. -P., Liu, Y. -H., Xing, X., Runov, A., Artemyev, A., and Zhang, X., (2020). An event study of simultaneous earthward and tailward reconnection exhaust flows in the Earth's midtail, Journal of Geophysical Research: Space Physics, 125, e2019JA027406, https://doi.org/10.1029/2019JA027406.

Wang, H., H. Lühr, and S. -Y. Ma (2005), Solar zenith angle and merging electric field control of field-aligned currents: A statistical study of the Southern Hemisphere, Journal of Geophysical Research: Space Physics, 110, A03306, doi:10.1029/2004JA010530.

Watanabe, M., S. Sakito, T. Tanaka, H. Shinagawa, and K. T. Murata (2014), Global MHD modeling of ionospheric convection and field-aligned currents associated with IMF By triggered theta auroras, Journal of Geophysical Research: Space Physics, 119, 6145–6166, doi:10.1002/2013JA019480.

Wei, Y., Pu, Z. -Y., Zong, Q. -G., Wan, W.-X., Ren, Z. -P., Fraenz, M., Dubinin, E., Tian, F., Shi, Q. -Q., Fu, S. -Y., Hong, M. -H., Oxygen escape from the Earth during geomagnetic reversals: Implications to mass extinction, Earth Planet. Sci. Lett., 394, 94-98, (2014).

Zhu, L., Schunk, R. W., and Sojka, J. J. (1997), Polar cap arcs: A review, J. Atmos. Sol.-Terr. Phys, 59, 10, 1087 – 1126.

Figures and Captions

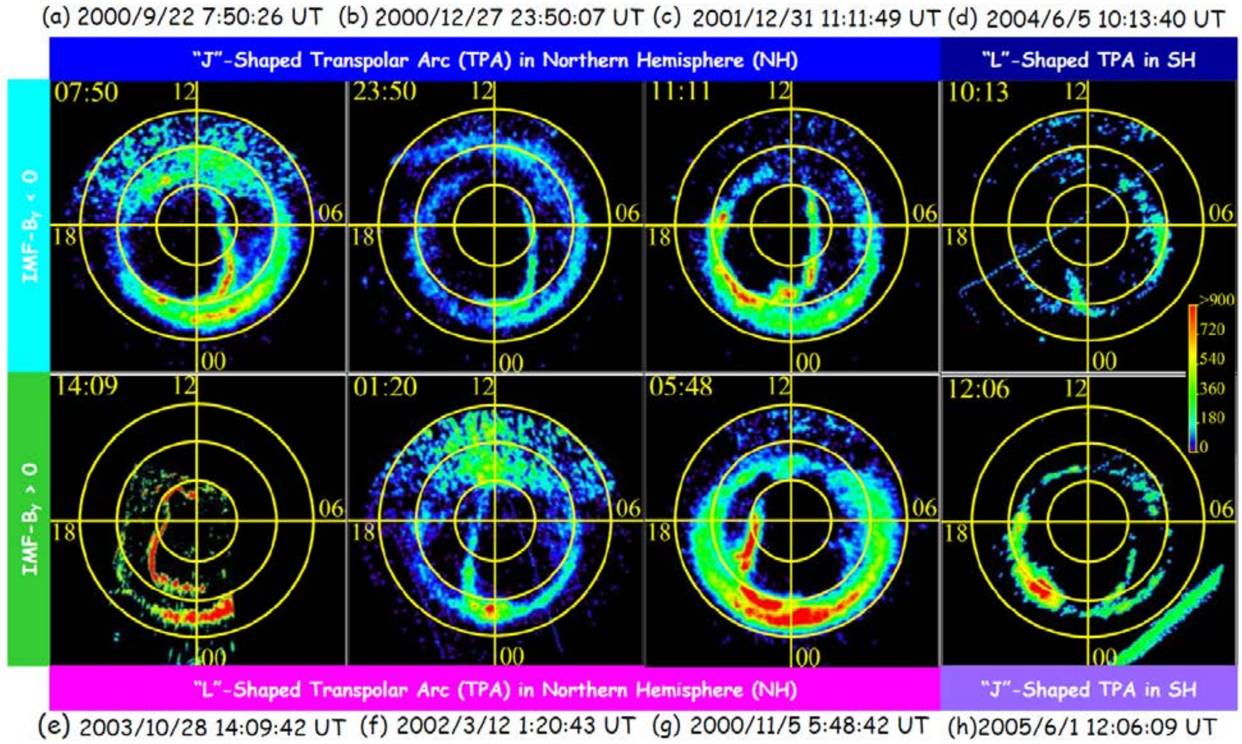

Figure 1: IMAGE-FUV-WIC data plots of selected 8 nightside distorted TPAs are shown. The upper panels (a) to (c) display the "J"-shaped TPAs whose nightside ends are distorted toward midnight or pre-midnight, observed in the Northern Hemisphere under negative (dawnward) IMF-B_y conditions. Panels (e) to (g) show the "L"-shaped TPAs with the nightside ends distorted toward midnight or post-midnight during positive (duskward) IMF-B_y intervals. Panels (d) and (h) show an "L"-shaped, and a "J"-shaped TPAs in the Southern Hemisphere during negative and positive IMF-B_y intervals. These panels are orientated in the same way, with noon (midnight) at the top (bottom), and dusk (dawn) on the left (right) of each plot. The yellow concentric circles show the magnetic latitude (MLat) from 60 degrees to 80 degrees. The color code is assigned according to Analogic-Digital Units (ADU), which is comparable to a detector count rate, being proportional to the observed auroral brightness (accounting for the spectral response of the instrument).

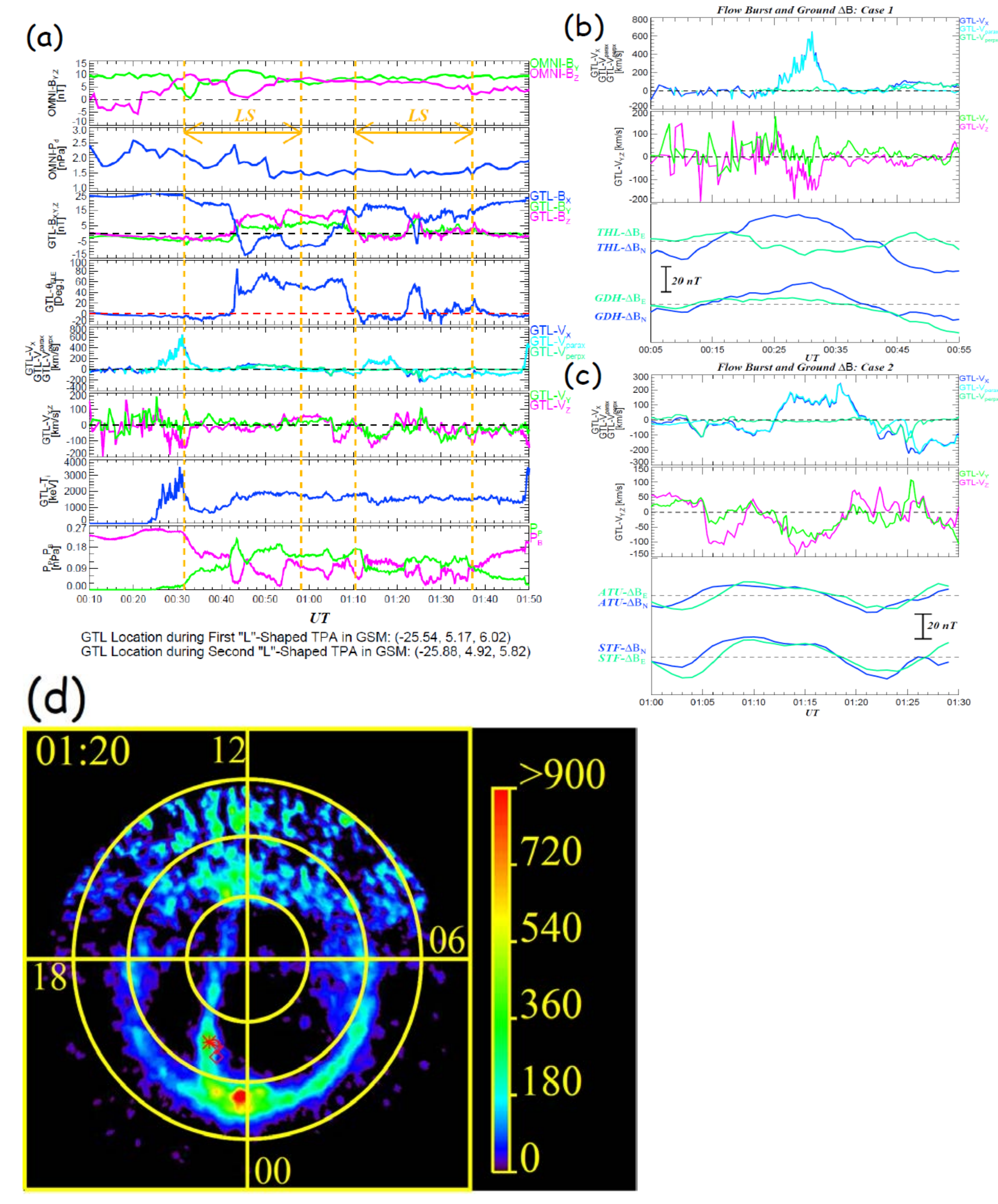

Figure 2: The summary plots of in-situ solar wind, duskside magnetotail and corresponding ground-based magnetic field observations, and the footpoints of the Geotail orbit projected onto the IMAGE FUV-WIC data on 12th March 2002 are displayed. Panel (a) shows a summary plot of OMNI-solar wind and Geotail magnetic field and plasma data in the duskside magnetotail during a 1 h 40 minute interval from 0:10 UT to 1:50 UT. The panels from top to bottom show the IMF-

B_y and $-B_z$ components in GSM coordinates, solar wind dynamic pressure, the three components of the duskside magnetotail magnetic field in GSM, associated magnetic field elevation angle, GSM-X and x-directional components of the plasma flow velocity parallel and perpendicular to the local magnetic field, the GSM-Y and -Z components of the magnetotail plasma velocity, the plasma (ion) temperature, and magnetic and plasma pressures, respectively. Two clear intensified intervals of the “L”-shaped TPA are each bracketed with two gold broken lines. Zoomed-in plasma flow velocity in GSM-X and x-directional components of parallel and perpendicular to the local magnetic field, including significant V_x enhancements which suggest an earthward plasma flow burst, and corresponding geomagnetic field variations observed at two representative ground observatories close to the “L”-shaped TPAs are shown in panels (b) and (c). The geomagnetic field fluctuations are calculated by a subtraction of the magnetic field average during the presented interval from the observed magnetic field data. Panel (d) shows the footpoints of the Geotail trajectory during 1 hour 40 minutes from 0:10 UT (asterisk) to 1:50 UT (diamond), projected onto the IMAGE FUV-WIC data observed on 1:20 UT, using the Tsyganenko 96 magnetic field empirical model (Tsyganenko and Stern, 1996).

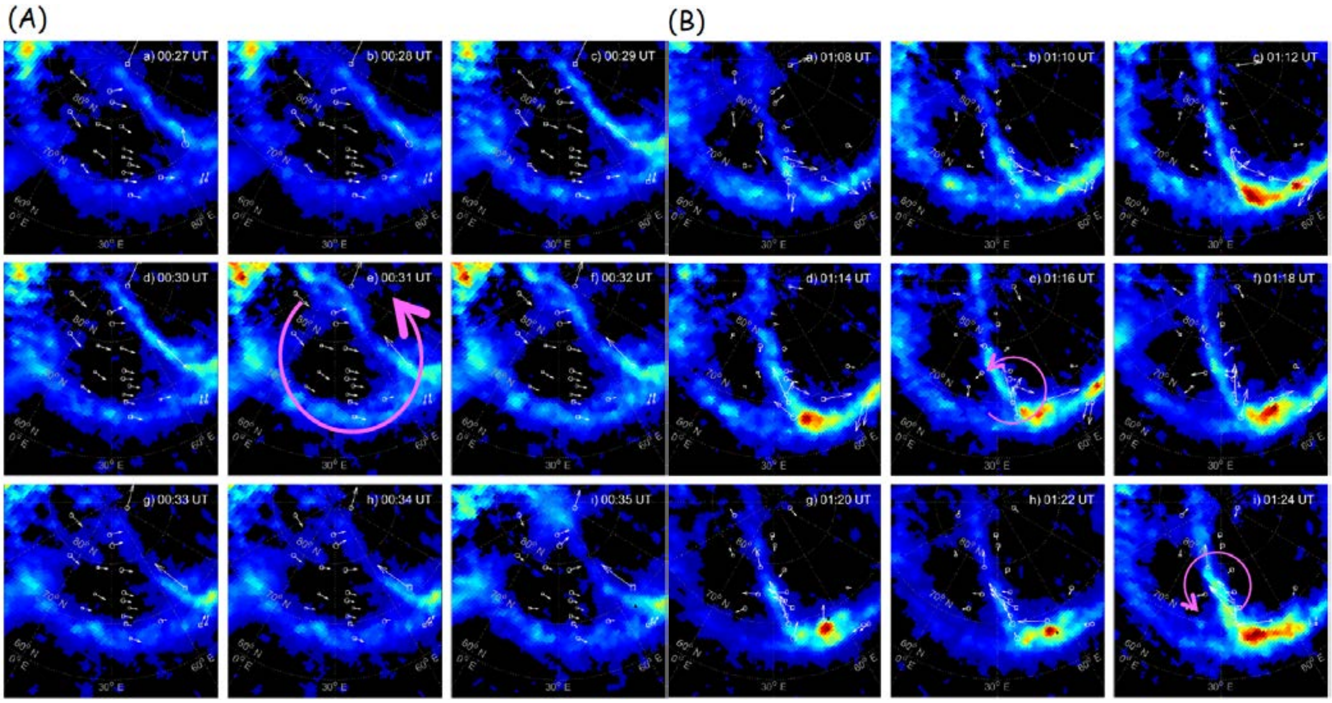

Figure 3: The vortex-like electric current structures detected by ground magnetic observatories beneath and in close proximity to the growth region of the "L"-shaped TPA from 00:27 UT to 00:35 UT with one minute time-step (panels A), and from 01:08 UT to 01:24 UT with two minutes time-step (panels B) on 12th March 2002 are shown. The electric current vectors are derived based on the ground magnetic field fluctuations during the time intervals including the first (a) and second (b) plasma earthward flow bursts, projected onto IMAGE FUV-WIC data in geomagnetic coordinates. Squares and circles with different sizes denote the polarity (positive and negative) and scale of the vertical directional magnetic field fluctuation component (ΔB_Z). Magenta circle arrows denote large- and small-scale -clockwise current vortices as seen in panels A and B, respectively.

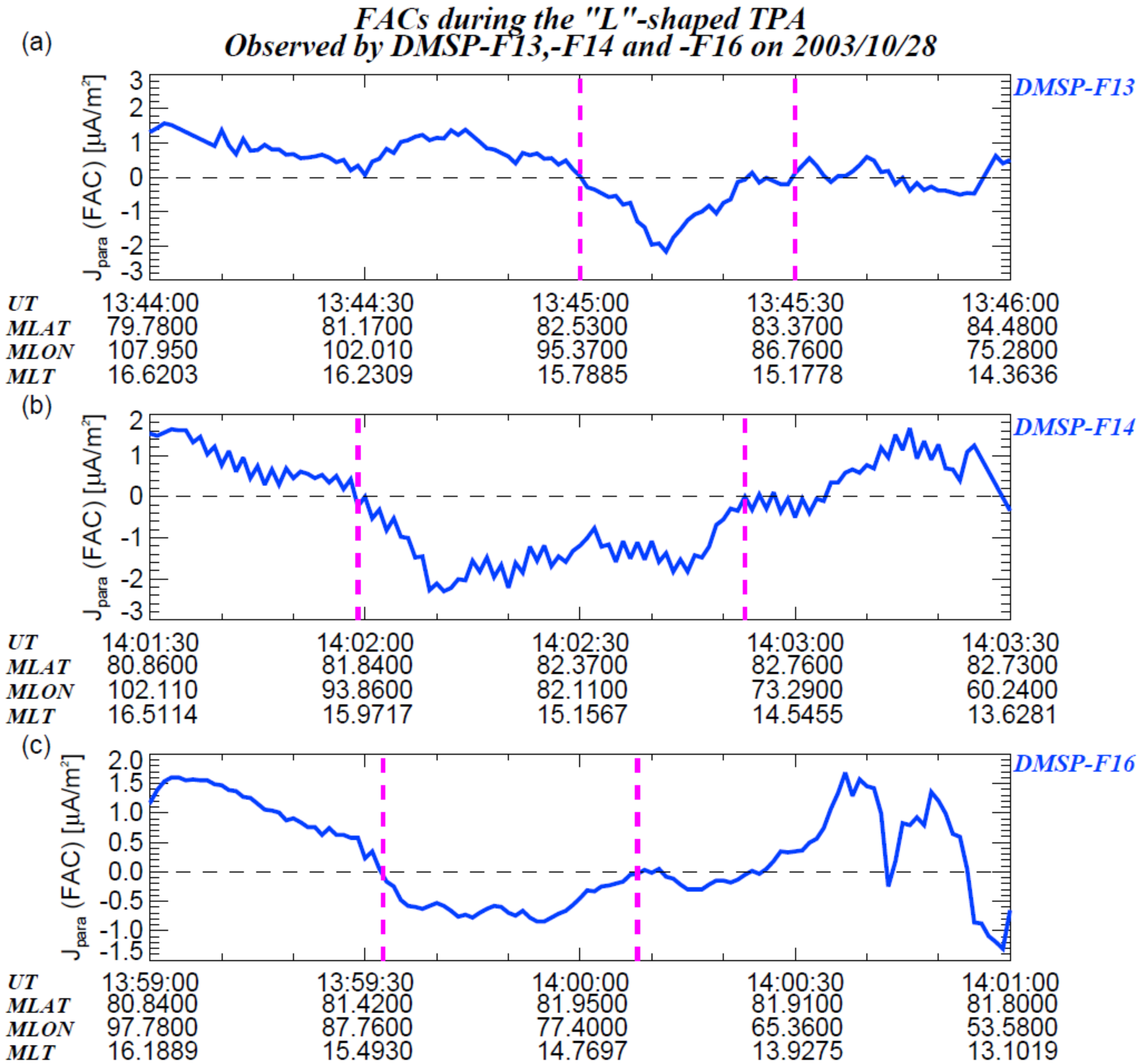

Figure 4: The temporal variations of the current density along the magnetic field lines (J_{para}, i.e., field-aligned current: FAC) against the universal time (UT), magnetic latitude (MLAT), magnetic longitude (MLON), and magnetic local time (MLT) are shown. All J_{para} values are derived from the magnetic field fluctuations observed during the DMSP-F13 (panel a) -F14 (panel b), and -F16 (panel c) crossings of the dayside straightforward bar-shaped part of the "L"-shaped TPA, observed on 28th October 2003. The detailed theory and methodology to deduce the J_{para} values from the magnetic field data are given in Wang et al. (2005) and Lühr et al. (2016). The TPA crossing time intervals of the three DMSP satellites are bracketed by two magenta broken lines.

(A)

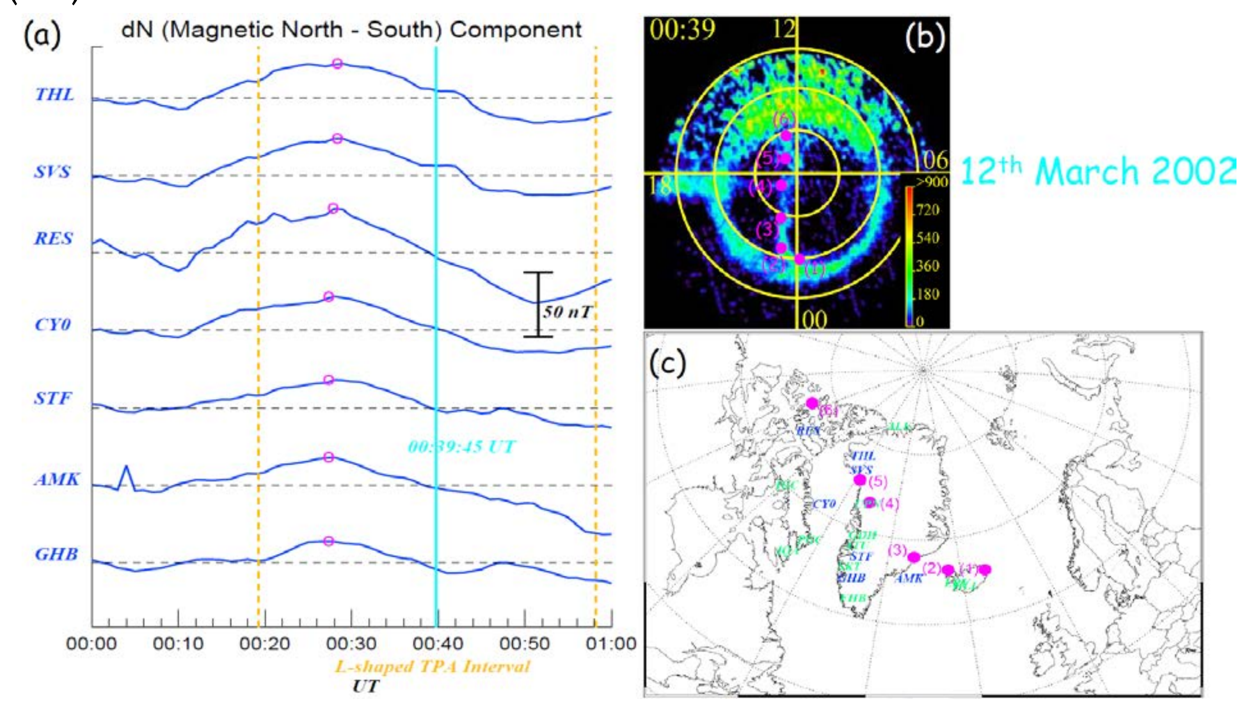

(B)

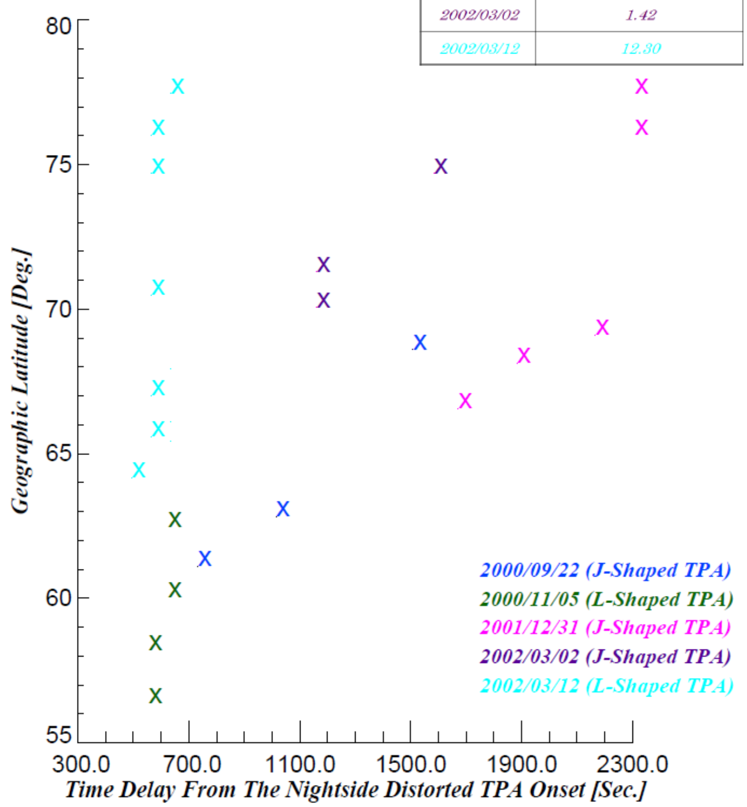

Event	Average Retreat Velocity [km/s]
2000/09/22	1.16
2000/11/05	7.30
2001/12/31	3.05
2002/03/02	1.42
2002/03/12	12.30

Figure 5: (A) The plots of in-situ geomagnetic magnetic field variations beneath and in close proximity to the growth regions of a nightside distorted TPA ("L"-shaped TPA observed on 12th March 2001) are displayed. Panels (a) to (c) show the magnetic field at several ground magnetic observatories corresponding to the locations beneath or in close proximity to the regions of growth of the "L"-shaped TPA. Several magenta points labelled with numbers in the IMAGE FUV-WIC plots (panel b) correspond to similarly labelled locations in geographical map (panel c). Panel (a) shows the plots of fluctuations in the local magnetic north-south magnetic field component (ΔB_N) at these observatories highlighted by blue. The fluctuation component, which was obtained by the subtraction of average magnetic field over the time interval of interest from the observed magnetic field values at each station, is plotted upon their averages (horizontal grey broken lines), and its peak during the "L"-shaped TPA intensification intervals (vertical gold broken lines), is marked by magenta open circle. The plots are sorted in decreasing order of latitude. The magnetic field fluctuation component at the time of panel (b) is indicated by a horizontal solid line in the panel. The color code of the IMAGE FUV-WIC data is assigned according to ADU. (B) The relationship between the magnetic peaks observed at several ground observatories beneath and in close proximity to the growth regions of the 5 nightside distorted TPAs from geographical low- to high-latitudes, and the time delays from the 5 TPA onset times to the magnetic peak times is shown. The magnetic field peaks seen in the local magnetic north-south magnetic field component (ΔB_N) are used. A rough estimation of the reconnection point retreat speed, which was calculated based on the slope of a line of geographical latitude versus the time delay between the magnetic peaks and the TPA onsets, is summarized in the table in the top-right of the panel. We adopted a value of 1 degree = 110.95 km to convert a unit of geographic latitude (degree) to equatorial distance (km).

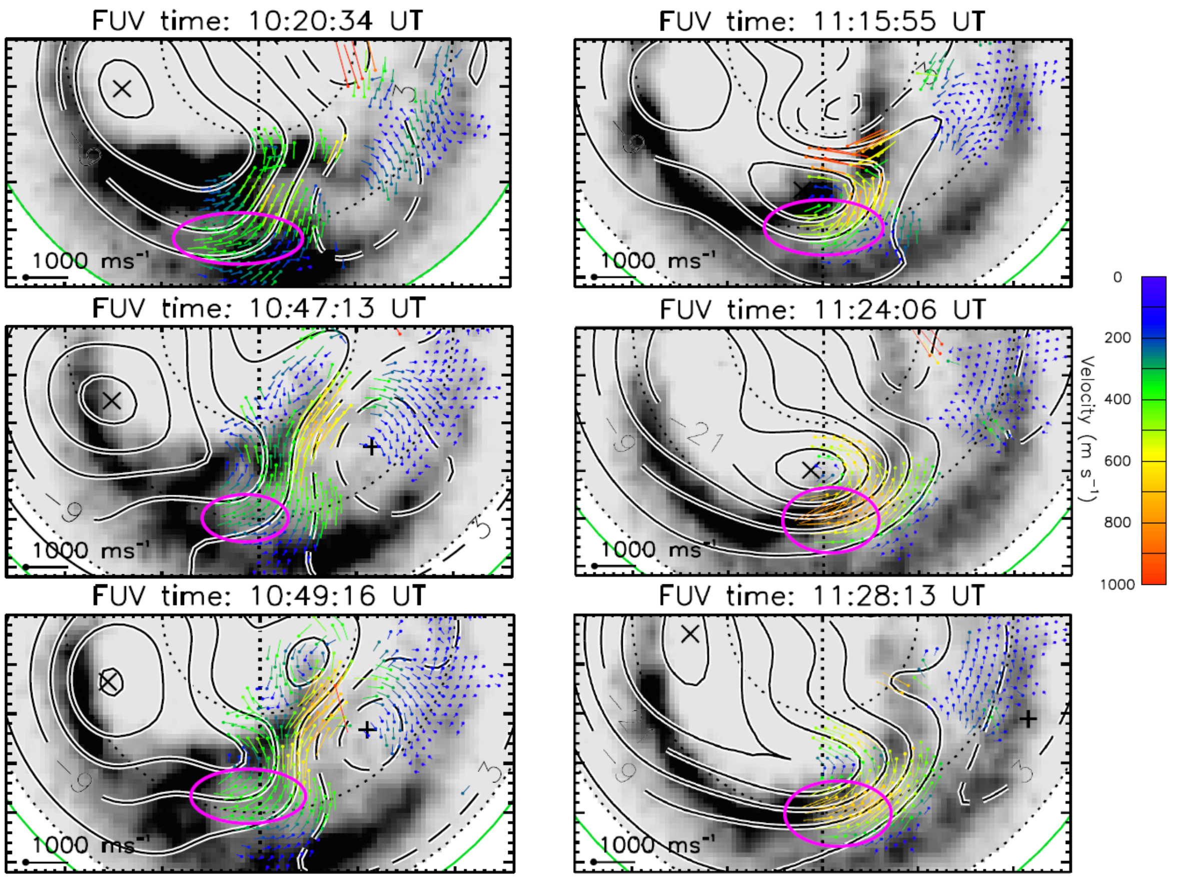

Figure 6: The nightside polar cap plasma flow streamlines and their line-of-sight velocity vectors measured by SuperDARN in the Northern Hemisphere, overlaid by the IMAGE FUV-WIC auroral image data, are shown. The dotted circles indicate the magnetic latitude (MLat) from 60 degrees to 80 degrees. The left, bottom and right sides in each panel show 18h, 24h and 6h in magnetic local time (MLT), respectively. The time resolutions of the SuperDARN and IMAGE FUV-WIC data are 2 minutes. These streamlines and velocity vectors are projected onto the geomagnetic grids, and positive (maximum denoted by a plus) and negative (minimum shown with a cross) electrostatic potential models, which are controlled by the IMF conditions, as shown with black solid and broken contours on dawn and dusk. The equipotential values are also overlaid. The green curves show the lower latitude limit of the plasma convection pattern in the polar cap (Heppner and Maynard, 1987), determined from the line-of-sight plasma velocities measured by the radars. Each dot shows a SuperDARN radar measurement. The length of the vectors and color code are assigned according to the flow orientation and speed in units of m/s. Westward "Tail Reconnection during IMF Northward and Non-substorm Interval" (TRINNI) flows are marked with magenta ovals.

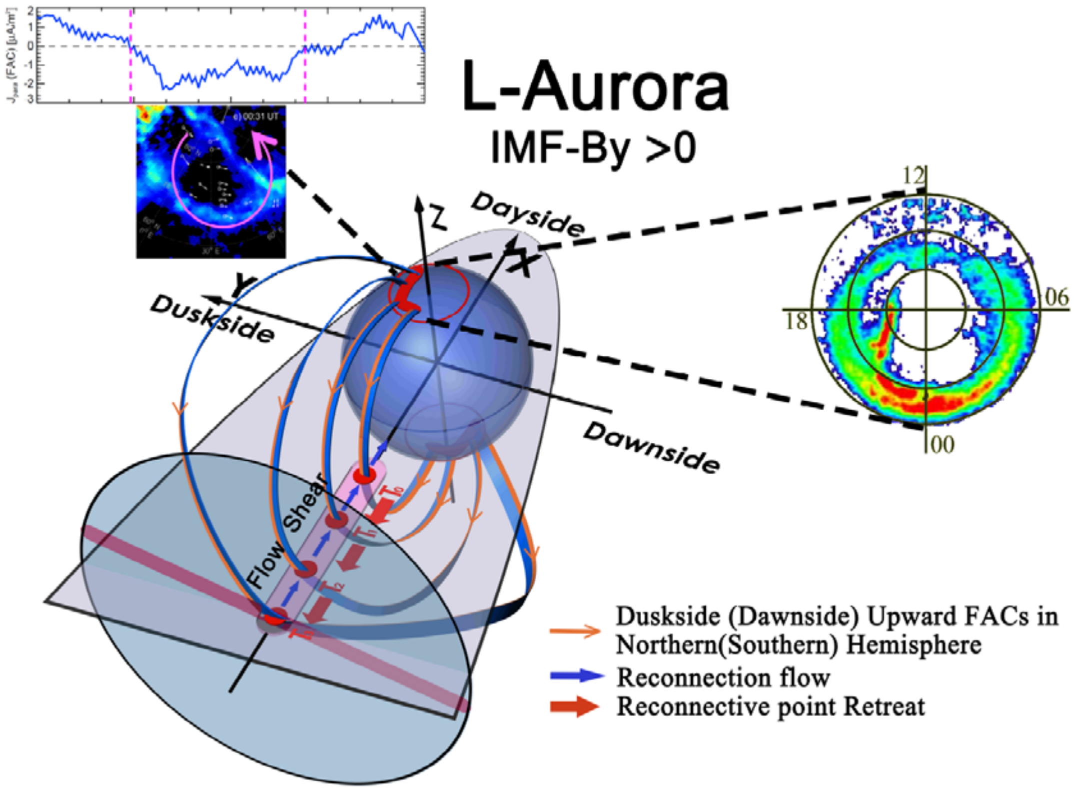

Figure 7: A schematic illustration showing a possible scenario for the formation of nightside distorted TPAs in terms of the magnetic field configuration changes, field-aligned currents (FACs), the magnetic reconnection plasma flows and the reconnection point retreats is shown. This illustration includes the observational examples of the "L"-shaped TPA, obtained by the IMAGE FUV-WIC on November 5th 2000, the counter-clockwise current vortex in close proximity to the "L"-shaped TPA on March 12th 2002, induced by FACs flowing out of the ionosphere, and direct measurement of upward FACs across the "L"-shaped TPA on October 28th 2003, detected by DMSP-F14. The magnetotail cross section and twisted plasma sheet are shown with a gray-shaded circle and red bar, respectively. FACs flowing toward magnetotail are indicated by orange curved arrows. Thin blue arrows show the fast plasma flows generated by magnetotail magnetic reconnection. The progressive retreat profile of the reconnection points (red dots) from T_0 to T_3 is shown with thick red arrows.

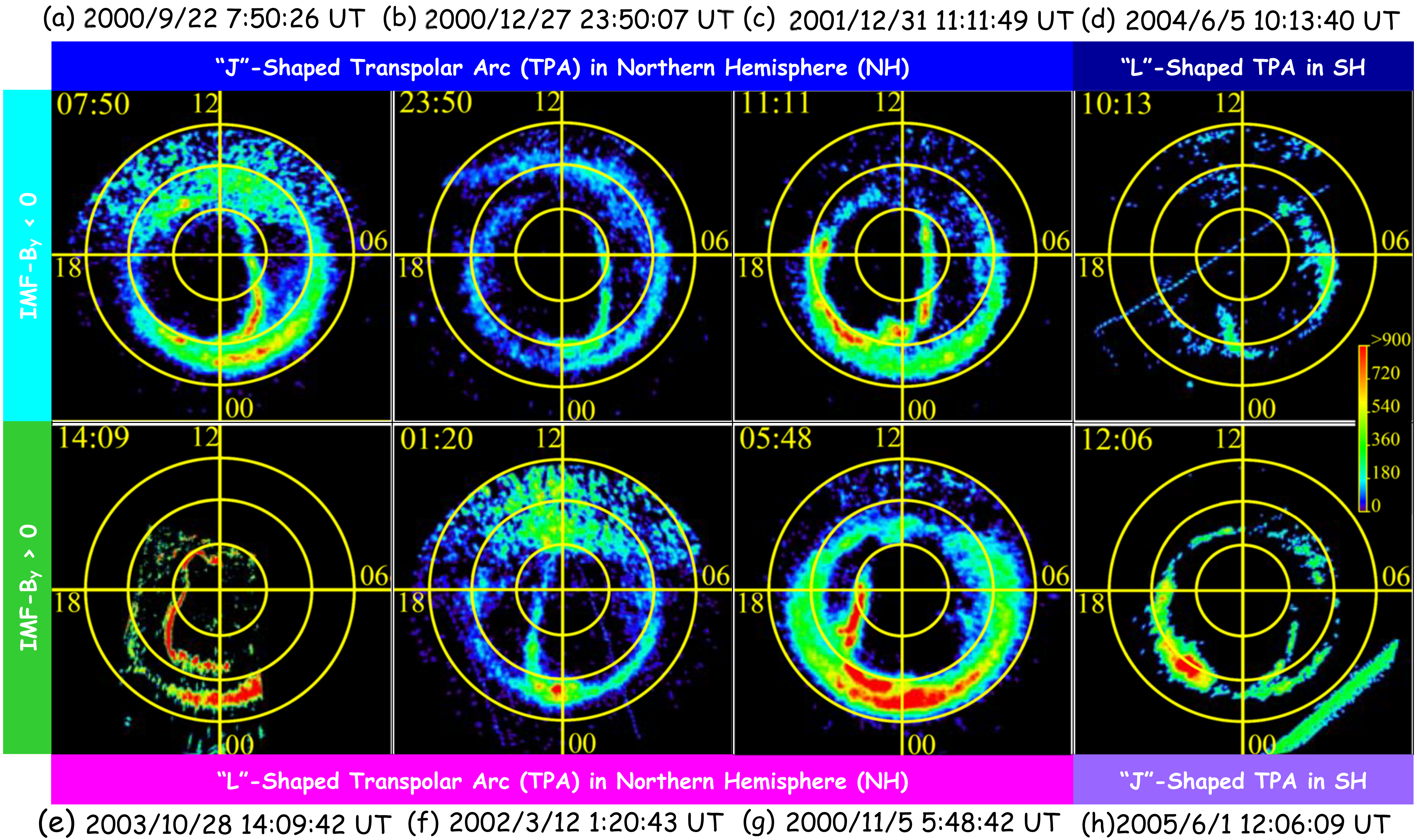

(a) 2000/9/22 7:50:26 UT
(b) 2000/12/27 23:50:07 UT
(c) 2001/12/31 11:11:49 UT
(d) 2004/6/5 10:13:40 UT
"J"-Shaped Transpolar Arc (TPA) in Northern Hemisphere (NH)
"L"-Shaped TPA in SH
IMF-By < 0
IMF-By > 0
07:50
23:50
11:11
10:13
14:09
01:20
05:48
12:06
12
06
18
00
>900
720
540
360
180
0
"L"-Shaped Transpolar Arc (TPA) in Northern Hemisphere (NH)
"J"-Shaped TPA in SH
(e) 2003/10/28 14:09:42 UT
(f) 2002/3/12 1:20:43 UT
(g) 2000/11/5 5:48:42 UT
(h)2005/6/1 12:06:09 UT

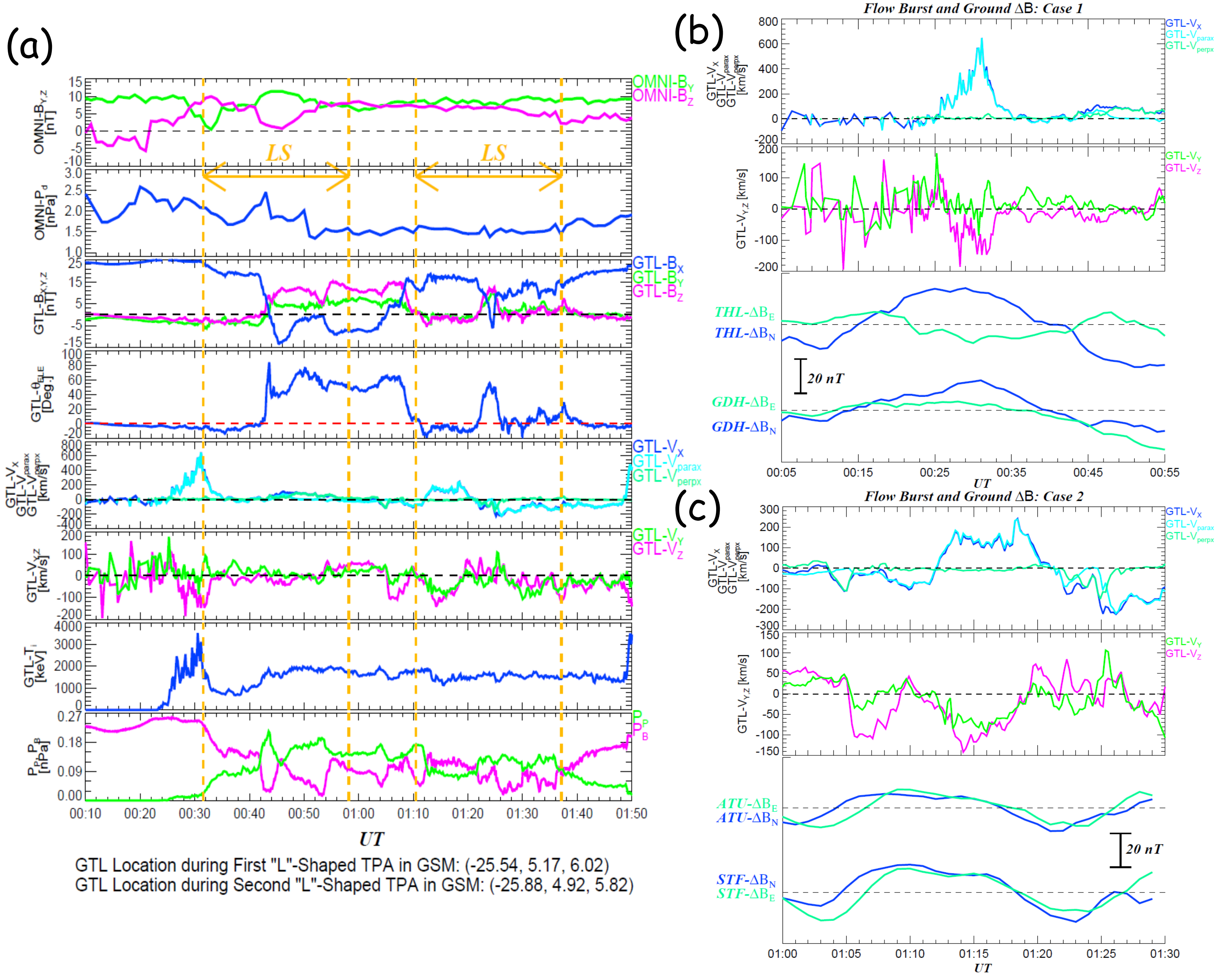

(a)
OMNI-B_Y,Z [nT]
OMNI-B_Y
OMNI-B_Z
LS
LS
OMNI-P_d [nPa]
GTL-B_X,Y,Z [nT]
GTL-B_X
GTL-B_Y
GTL-B_Z
GTL-θ_ELE [Deg.]
GTL-V_X
GTL-V_parax
GTL-V_perpx
[km/s]
GTL-V_Y,Z [km/s]
GTL-V_Y
GTL-V_Z
GTL-T_i [keV]
P_P, P_B [nPa]
P_P
P_B
00:10 00:20 00:30 00:40 00:50 01:00 01:10 01:20 01:30 01:40 01:50
UT
GTL Location during First "L"-Shaped TPA in GSM: (-25.54, 5.17, 6.02)
GTL Location during Second "L"-Shaped TPA in GSM: (-25.88, 4.92, 5.82)
(b)
Flow Burst and Ground ΔB: Case 1
GTL-V_X
GTL-V_parax
GTL-V_perpx
GTL-V_Y,Z [km/s]
GTL-V_Y
GTL-V_Z
THL-ΔB_E
THL-ΔB_N
20 nT
GDH-ΔB_E
GDH-ΔB_N
00:05 00:15 00:25 00:35 00:45 00:55
UT
(c)
Flow Burst and Ground ΔB: Case 2
GTL-V_X
GTL-V_parax
GTL-V_perpx
GTL-V_Y,Z [km/s]
GTL-V_Y
GTL-V_Z
ATU-ΔB_E
ATU-ΔB_N
20 nT
STF-ΔB_N
STF-ΔB_E
01:00 01:05 01:10 01:15 01:20 01:25 01:30
UT

(d)

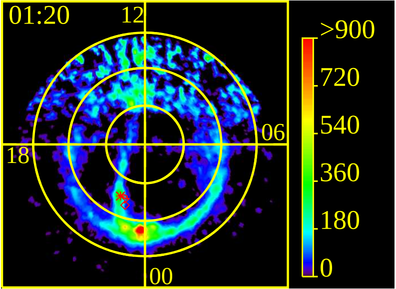

(A)

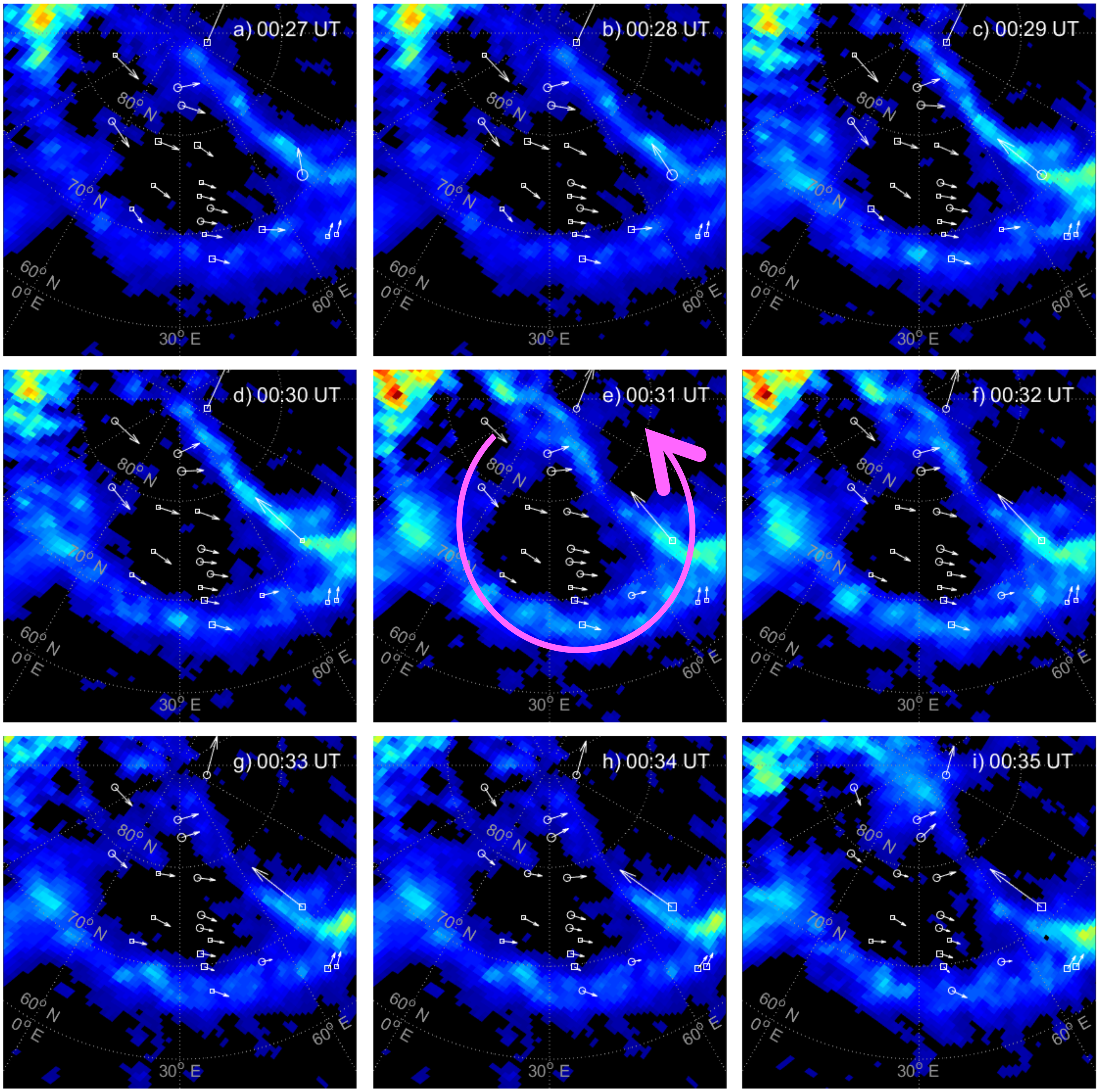
a) 00:27 UT
b) 00:28 UT
c) 00:29 UT
d) 00:30 UT
e) 00:31 UT
f) 00:32 UT
g) 00:33 UT
h) 00:34 UT
i) 00:35 UT
80° N
70° N
60° N
0° E
30° E
60° E

(B)

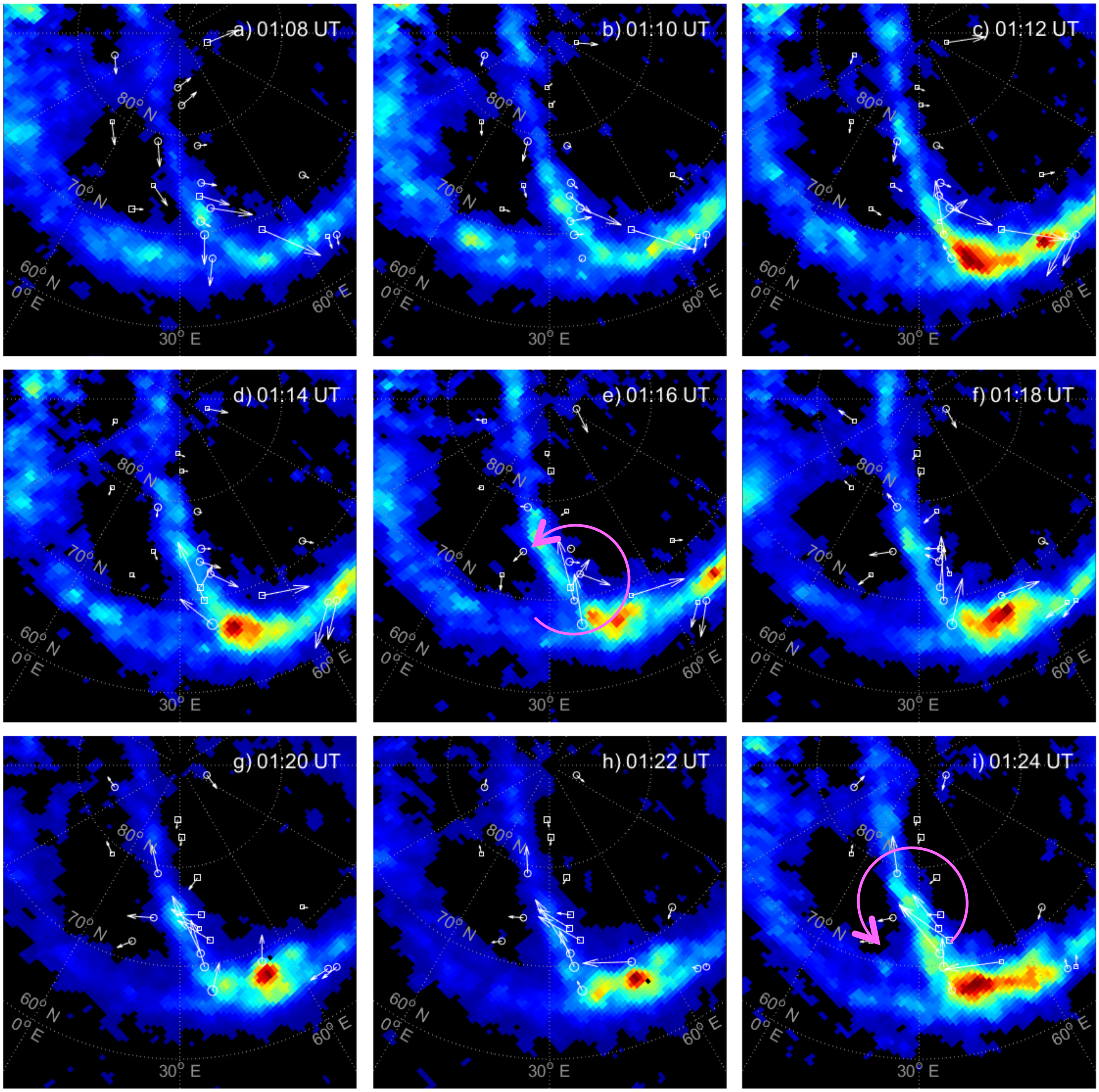

a) 01:08 UT
b) 01:10 UT
c) 01:12 UT
d) 01:14 UT
e) 01:16 UT
f) 01:18 UT
g) 01:20 UT
h) 01:22 UT
i) 01:24 UT
80° N
70° N
60° N
0° E
30° E
60° E

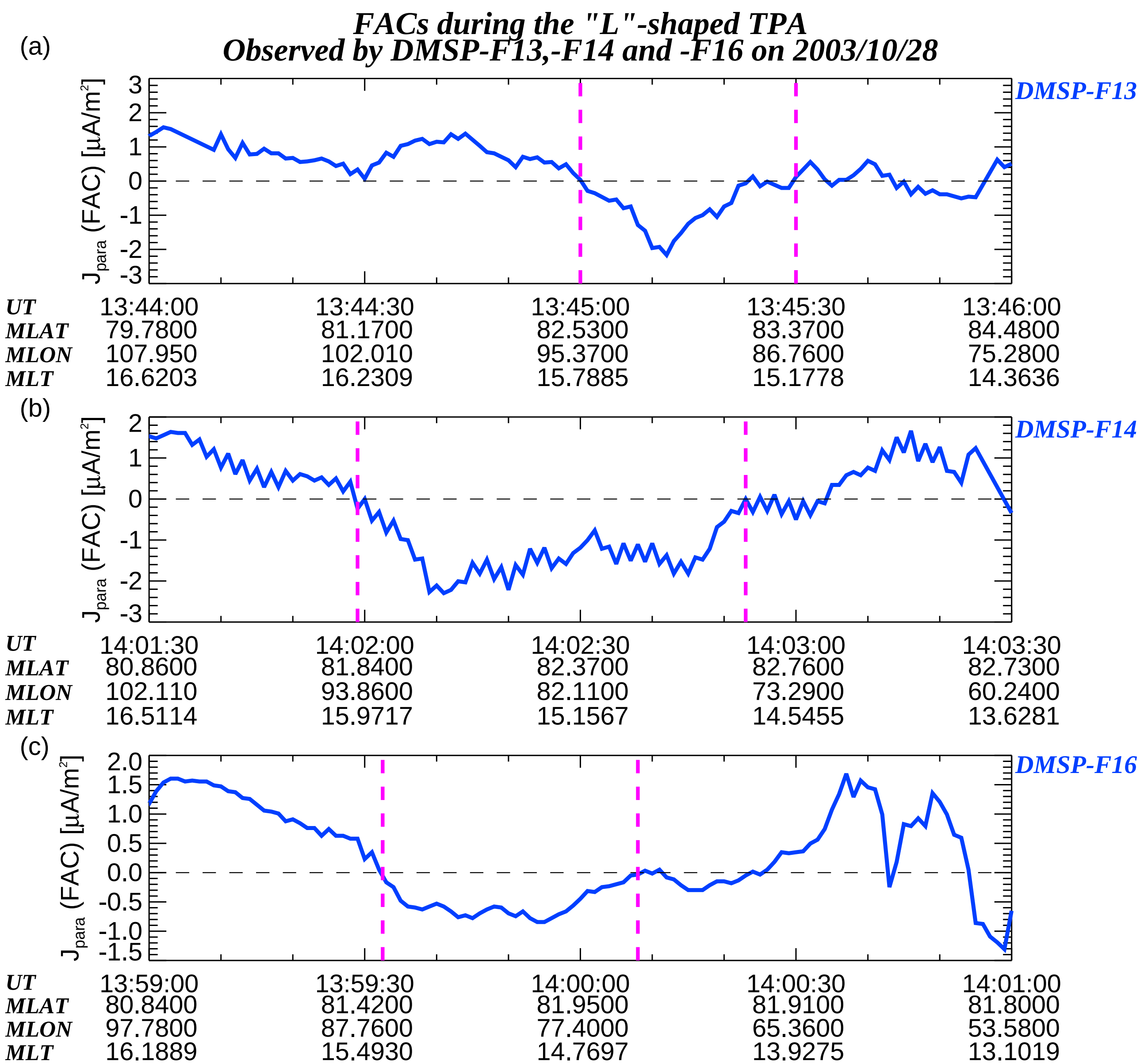

FACs during the "L"-shaped TPA
Observed by DMSP-F13,-F14 and -F16 on 2003/10/28
(a)
DMSP-F13
J_para (FAC) [µA/m²]
UT 13:44:00 13:44:30 13:45:00 13:45:30 13:46:00
MLAT 79.7800 81.1700 82.5300 83.3700 84.4800
MLON 107.950 102.010 95.3700 86.7600 75.2800
MLT 16.6203 16.2309 15.7885 15.1778 14.3636
(b)
DMSP-F14
J_para (FAC) [µA/m²]
UT 14:01:30 14:02:00 14:02:30 14:03:00 14:03:30
MLAT 80.8600 81.8400 82.3700 82.7600 82.7300
MLON 102.110 93.8600 82.1100 73.2900 60.2400
MLT 16.5114 15.9717 15.1567 14.5455 13.6281
(c)
DMSP-F16
J_para (FAC) [µA/m²]
UT 13:59:00 13:59:30 14:00:00 14:00:30 14:01:00
MLAT 80.8400 81.4200 81.9500 81.9100 81.8000
MLON 97.7800 87.7600 77.4000 65.3600 53.5800
MLT 16.1889 15.4930 14.7697 13.9275 13.1019

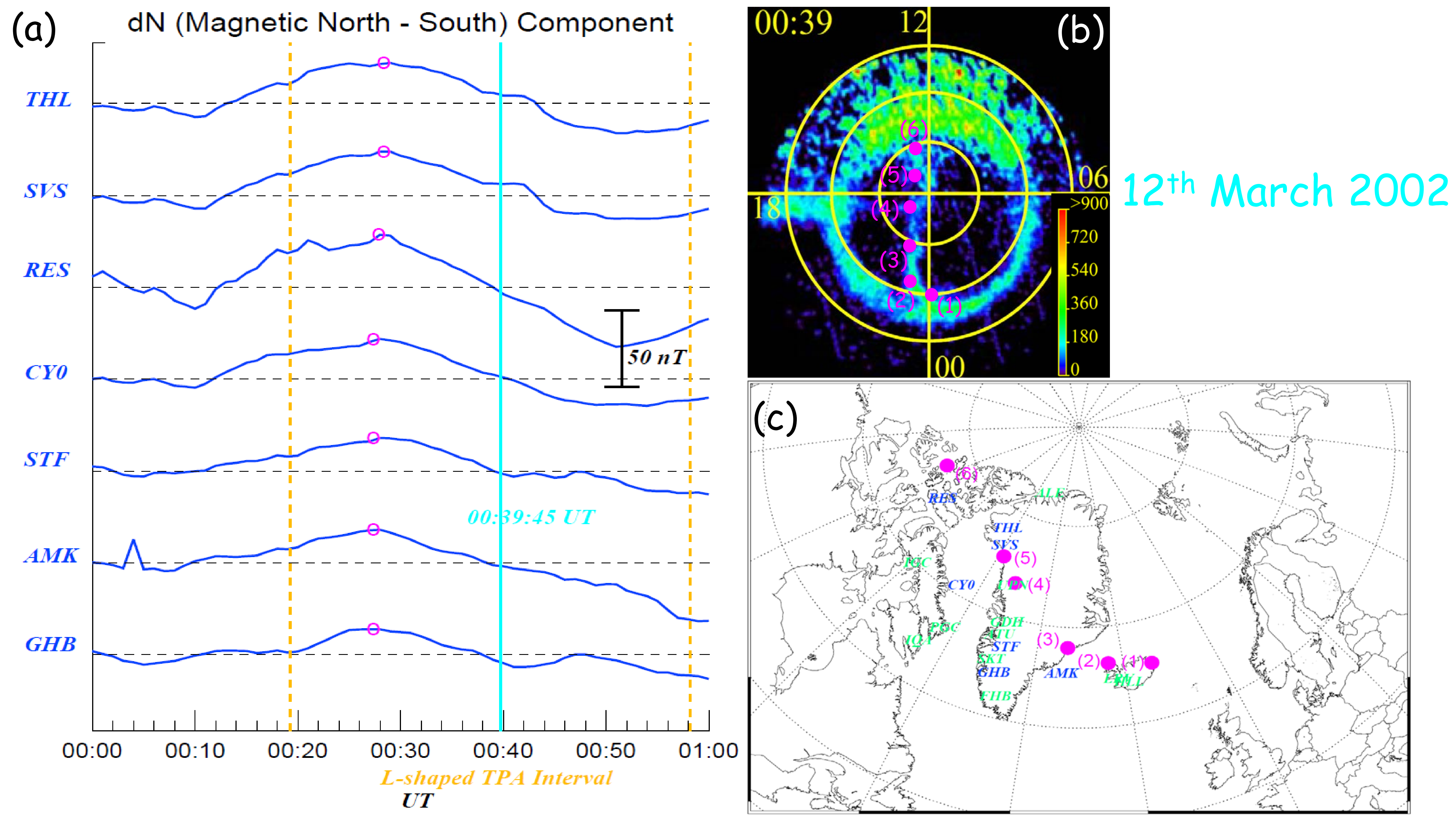

(a)
dN (Magnetic North - South) Component
THL
SVS
RES
CY0
STF
AMK
GHB
50 nT
00:39:45 UT
00:00
00:10
00:20
00:30
00:40
00:50
01:00
L-shaped TPA Interval
UT
(b)
00:39
12
06
18
00
>900
720
540
360
180
0
(6)
(5)
(4)
(3)
(2)
(1)
12th March 2002
(c)
(6)
RES
ALE
THL
SVS
(5)
CY0
(4)
GDH
STF
(3)
(2)
(1)
SKT
GHB
AMK
FHB

Event	*Average Retreat Velocity [km/s]*
2000/09/22	*1.16*
2000/11/05	*7.30*
2001/12/31	*3.05*
2002/03/02	*1.42*
2002/03/12	*12.30*

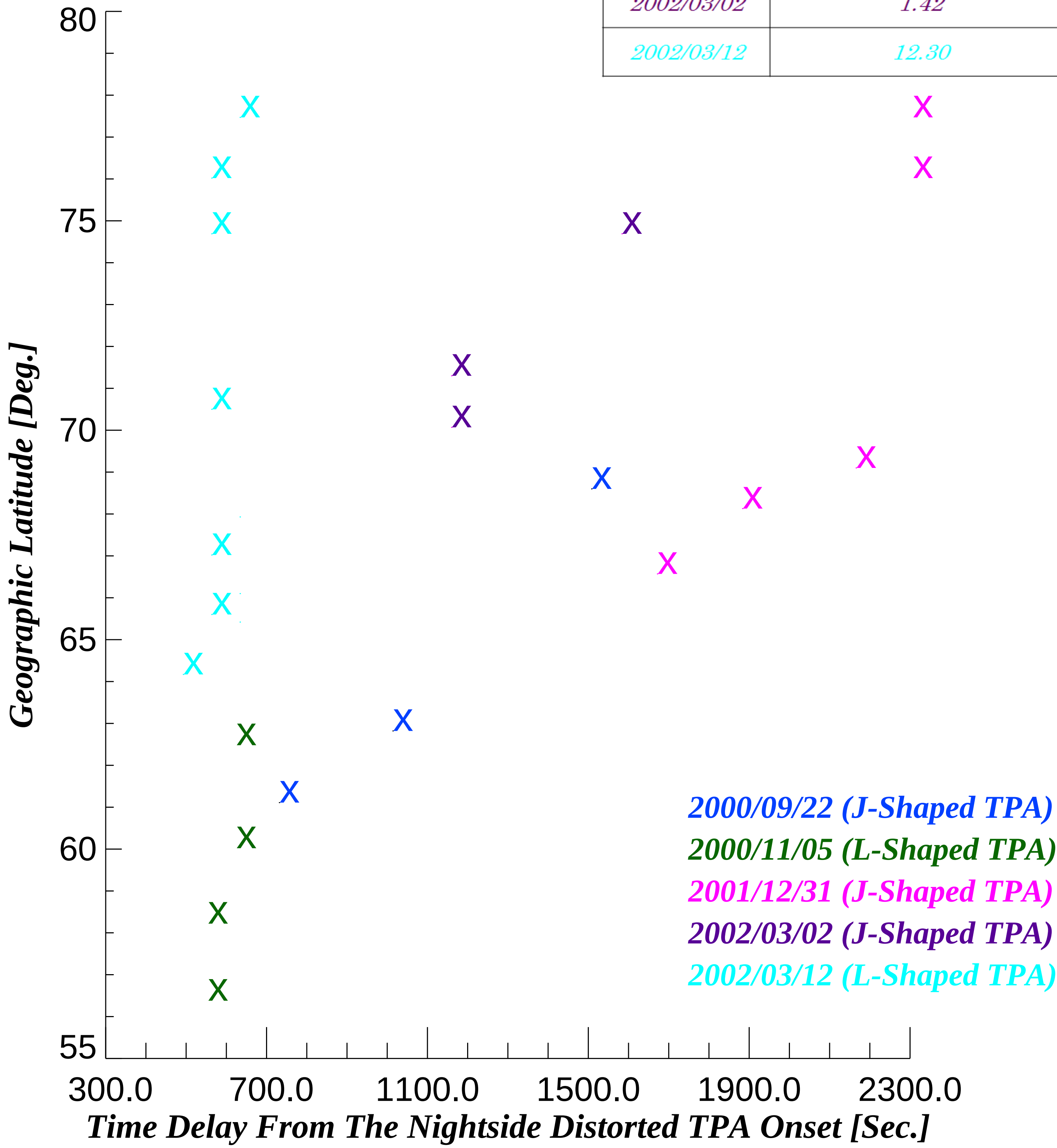

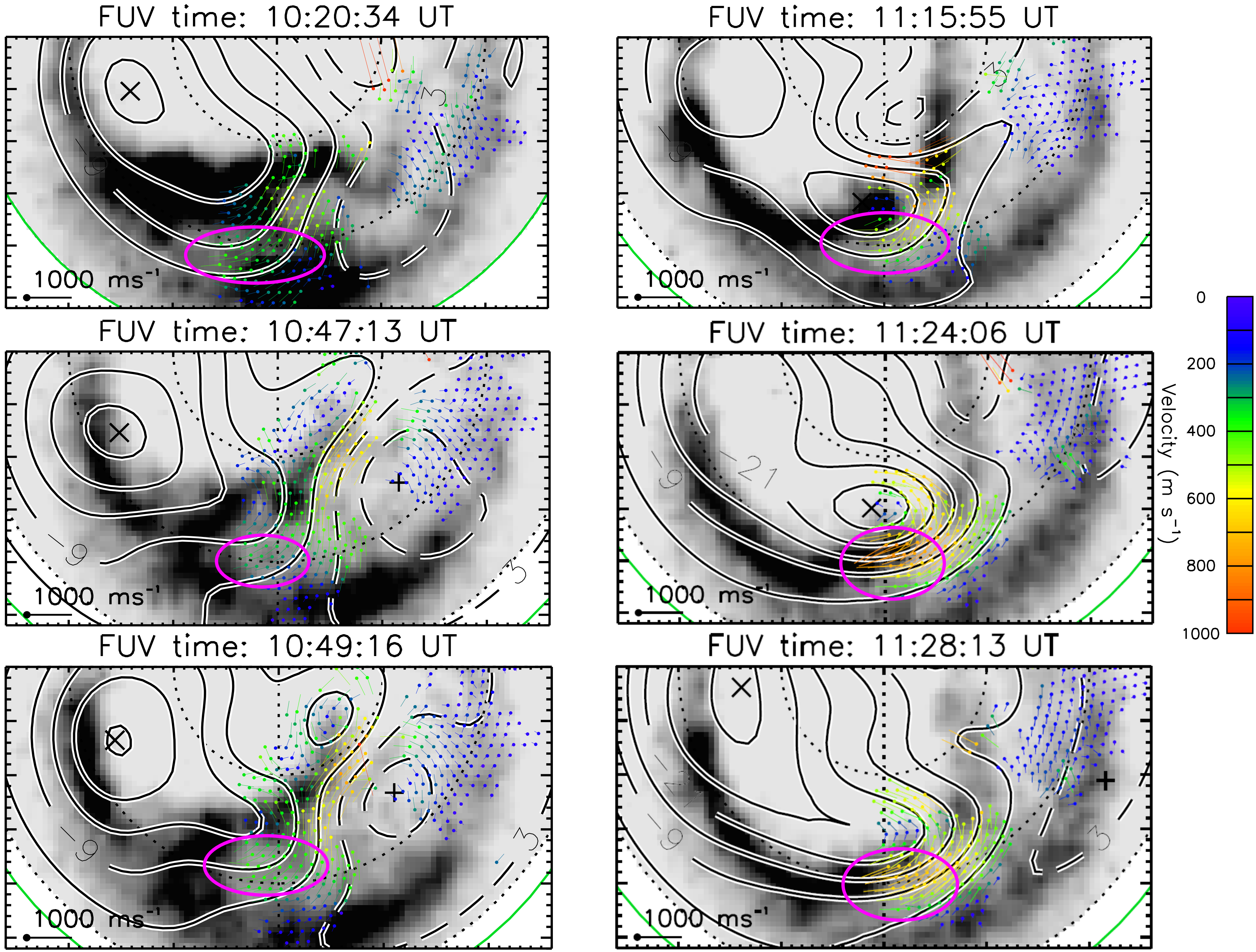

FUV time: 10:20:34 UT
FUV time: 11:15:55 UT
FUV time: 10:47:13 UT
FUV time: 11:24:06 UT
FUV time: 10:49:16 UT
FUV time: 11:28:13 UT
1000 ms⁻¹
Velocity (m s⁻¹)
0
200
400
600
800
1000

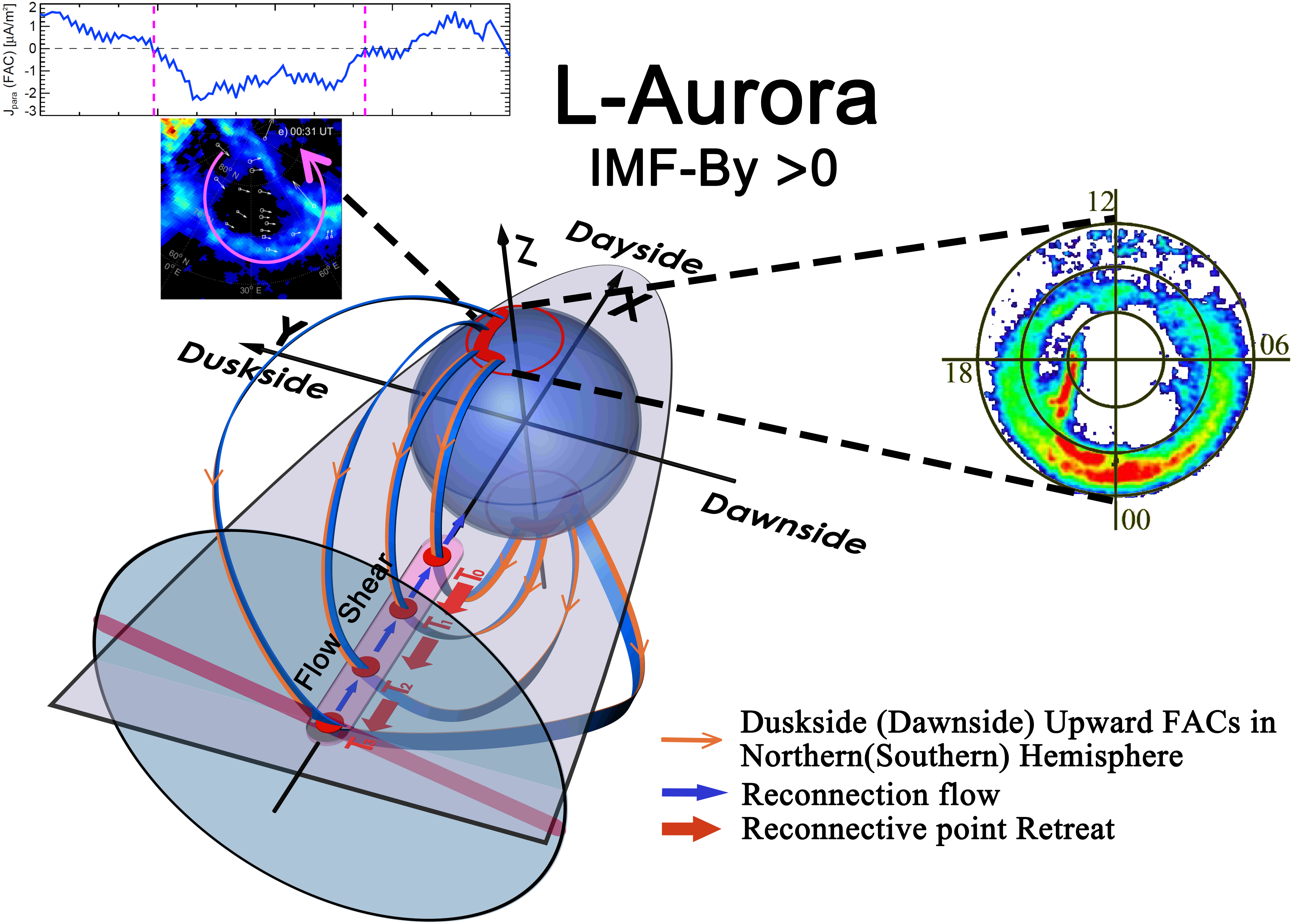

L-Aurora
IMF-By >0
J_{para} (FAC) [μA/m²]
e) 00:31 UT
80° N
70°
60° N
0° E
30° E
60° E
Z
X
Y
Dayside
Duskside
Dawnside
12
06
18
00
Flow Shear
T_0
T_1
T_2
T_3
Duskside (Dawnside) Upward FACs in Northern(Southern) Hemisphere
Reconnection flow
Reconnective point Retreat

Journal of Geophysical Research: Space Physics

Supporting Information for

North-south Asymmetric Nightside Distorted Transpolar Arcs within A Framework of Deformed Magnetosphere-Ionosphere Coupling: IMF-B_y Dependence, Ionospheric Currents, and Magnetotail Reconnection

Motoharu Nowada[1], Qiu-Gang Zong[2], Benoît Hubert[3], Quan-Qi Shi[1], Yong-Fu Wang[2], Jun Yang[1], Adrian Grocott[4], Alexander W. Degeling[1], An-Min Tian[1], Xu-Zhi Zhou[2], and Chao Yue[2]

1. Shandong Provincial Key Laboratory of Optical Astronomy and Solar-Terrestrial Environment, Institute of Space Sciences, Shandong University, Weihai, People's Republic of China.

2. Institute of Space Physics and Applied Technology, School of Earth and Space Sciences, Peking University, People's Republic of China.

3. Space science, Technologies and Astrophysics Research (STAR) Institute, Université de Liège, Belgium.

4. Space and Planetary Physics Group, Department of Physics, Lancaster University, Lancaster, UK.

Contents of this file

Figures S1 to S4
Tables S1 to S2

Introduction

The 5 auroral imager snapshots of the temporal evolutions of the 4 nightside distorted TPAs and corresponding IMF and solar wind plasma conditions are shown in Figure S1. The IMF and solar wind plasma parameters were obtained through the measurements of ACE and Geotail. In the auroral imager data, the optical noises such as the dayglow contaminations were removed using the same techniques as the noise removals in the auroral imager data shown in Figure 1. Figure S2 shows the plots of the magnetic field and plasma data taken from the Geotail measurements of the dawnside magnetotail on March 2nd, 2002, corresponding solar wind conditions, and the geomagnetic field perturbations measured at two representative ground magnetic observatories close to the "J"-shaped TPA. The plots of in-situ geomagnetic magnetic field variations beneath and in close proximity to the regions of growth of the 5 nightside distorted TPAs are displayed in Figure S3. The 4 consecutive auroral imager data during the time interval of the "L"-shaped TPA discussed in this paper (March 12th, 2002), and corresponding plots of the SuperDARN radar data are displayed in Figure S4. These figures show TPA-associated ionospheric current patterns as possible evidence for generations of upward and downward Field-aligned Currents (FACs).

2000/9/22 6:34:53 UT – 8:25:08 UT (IMAGE-FUV-WIC)

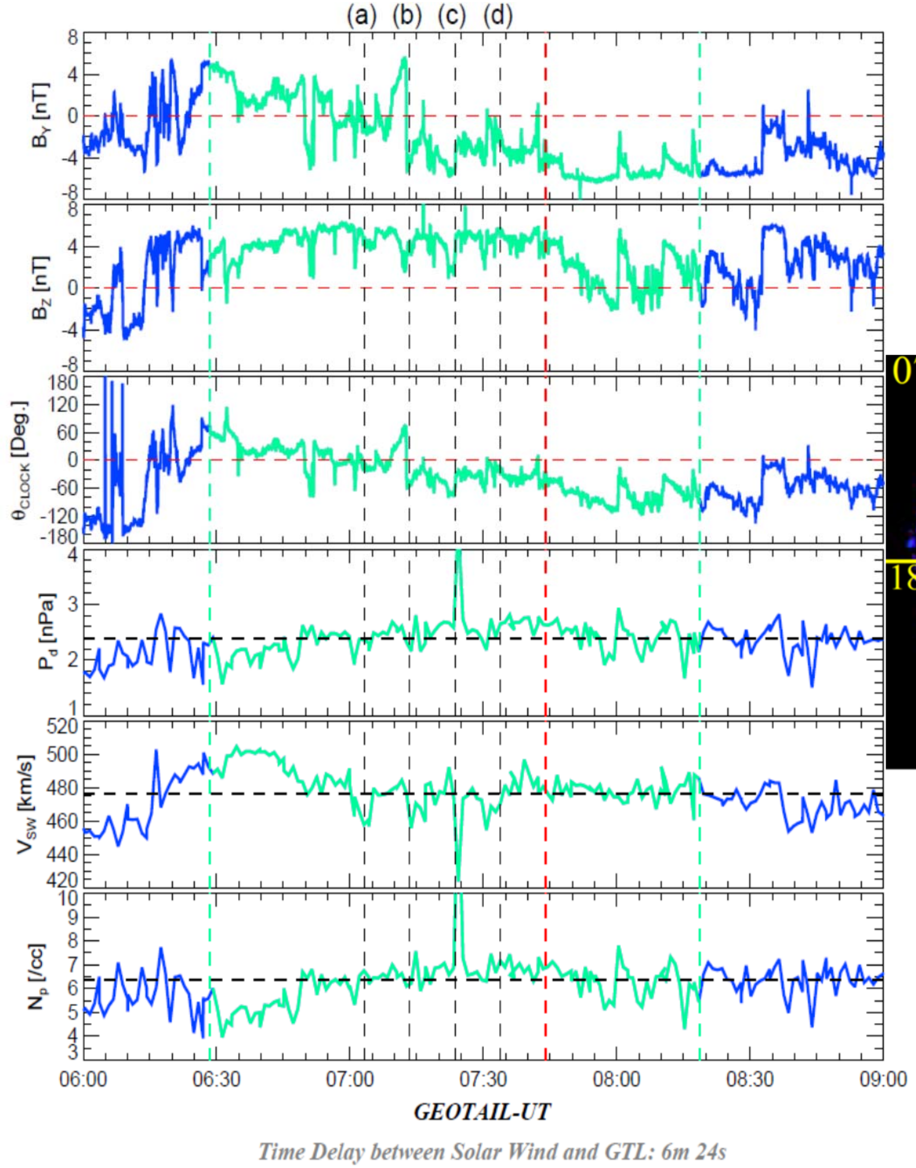

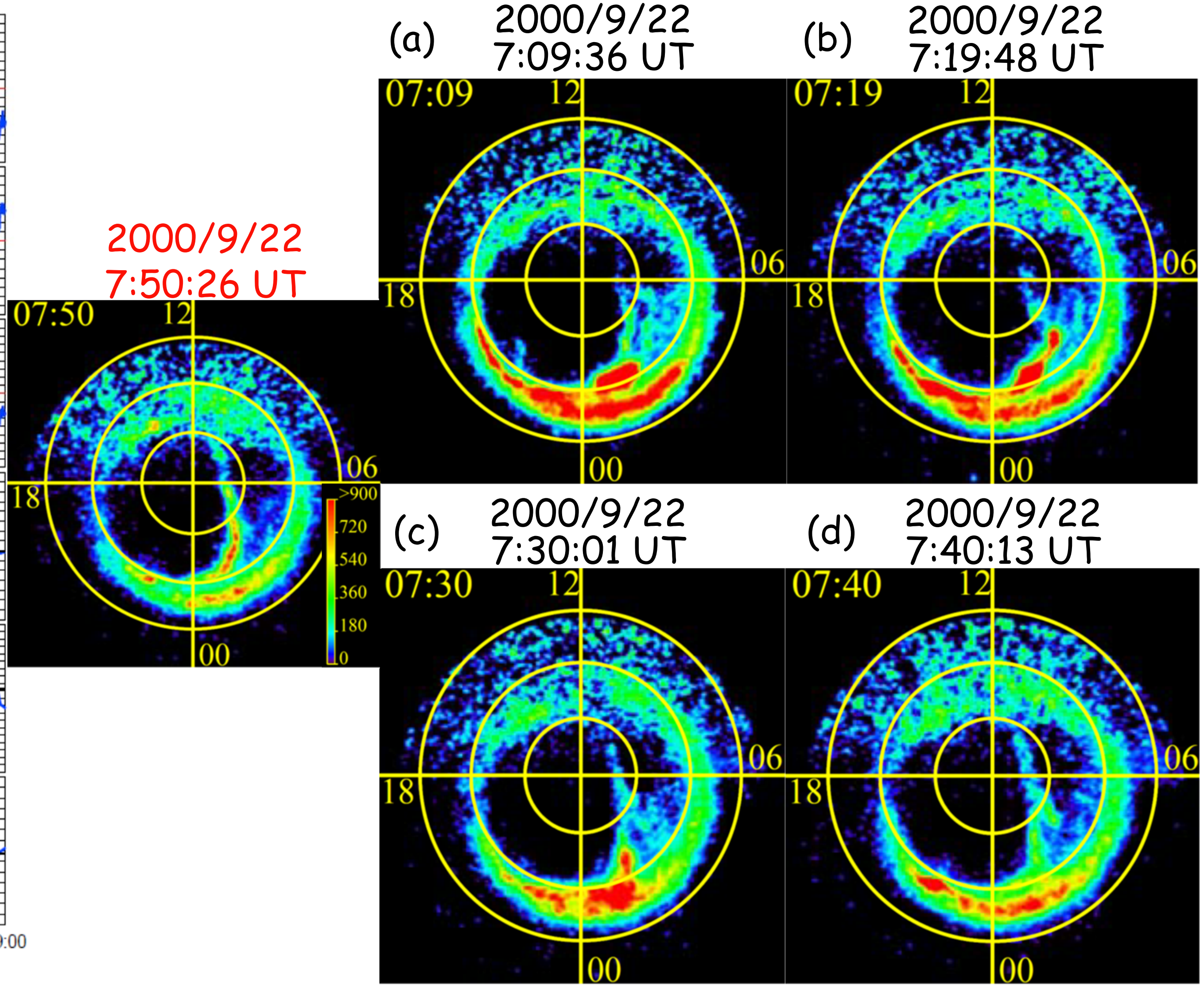

2000/11/5 5:34:24 UT – 7:08:24 UT (IMAGE-FUV-WIC)

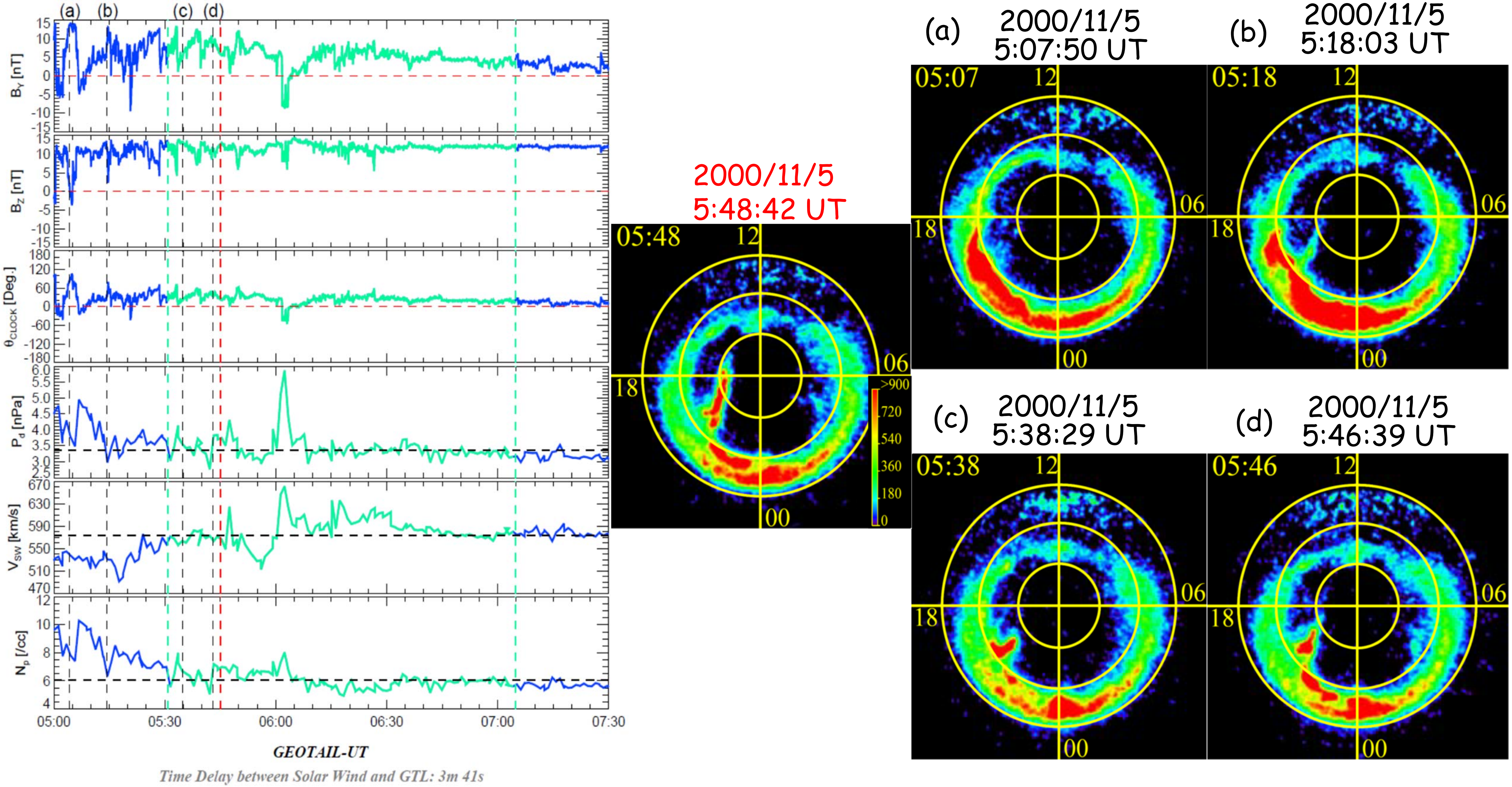

2001/12/31 10:20:34 UT - 14:40:46 UT (IMAGE-FUV-WIC)

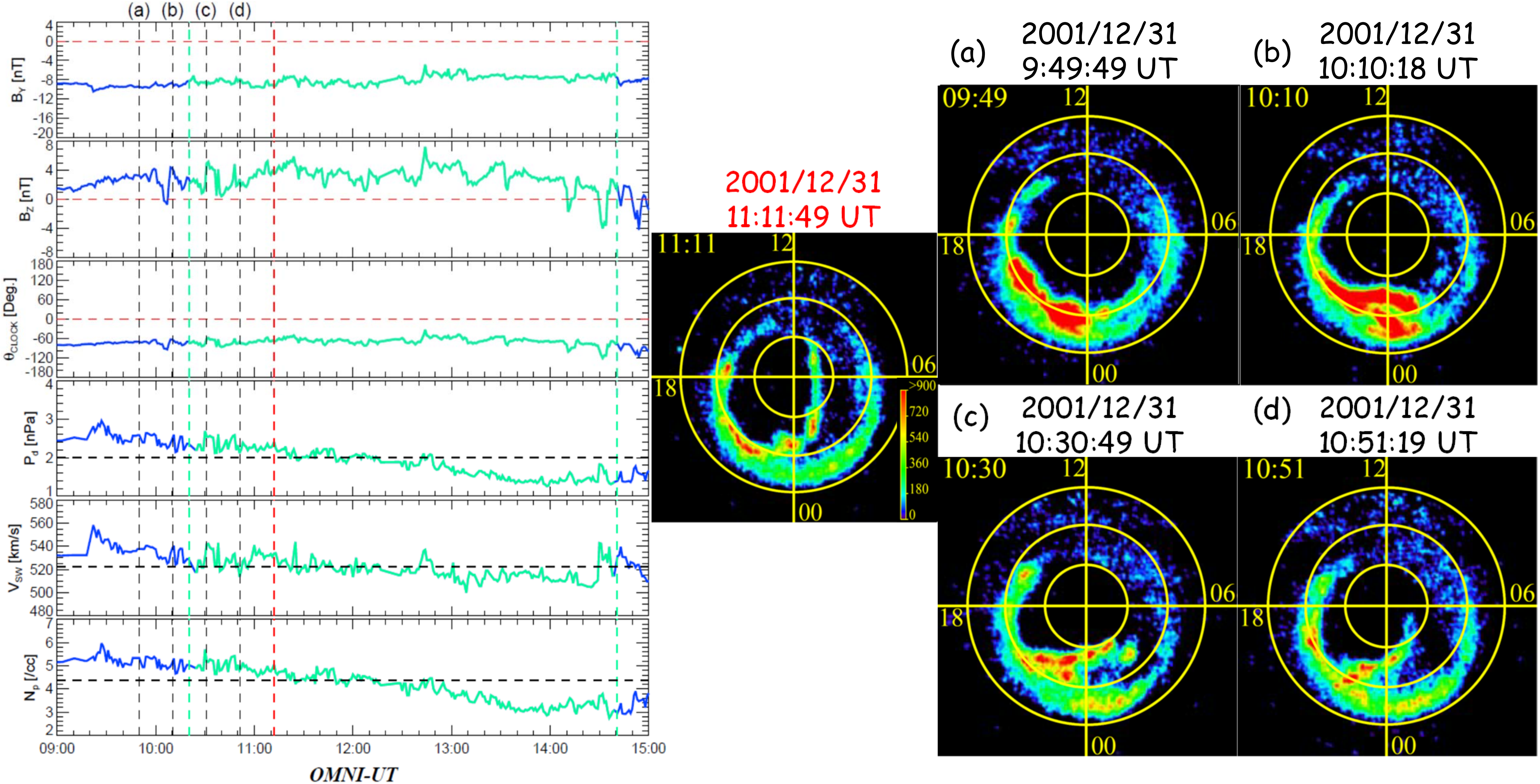

2003/10/28 13:20:28 UT – 14:17:55 UT (IMAGE-FUV-WIC)

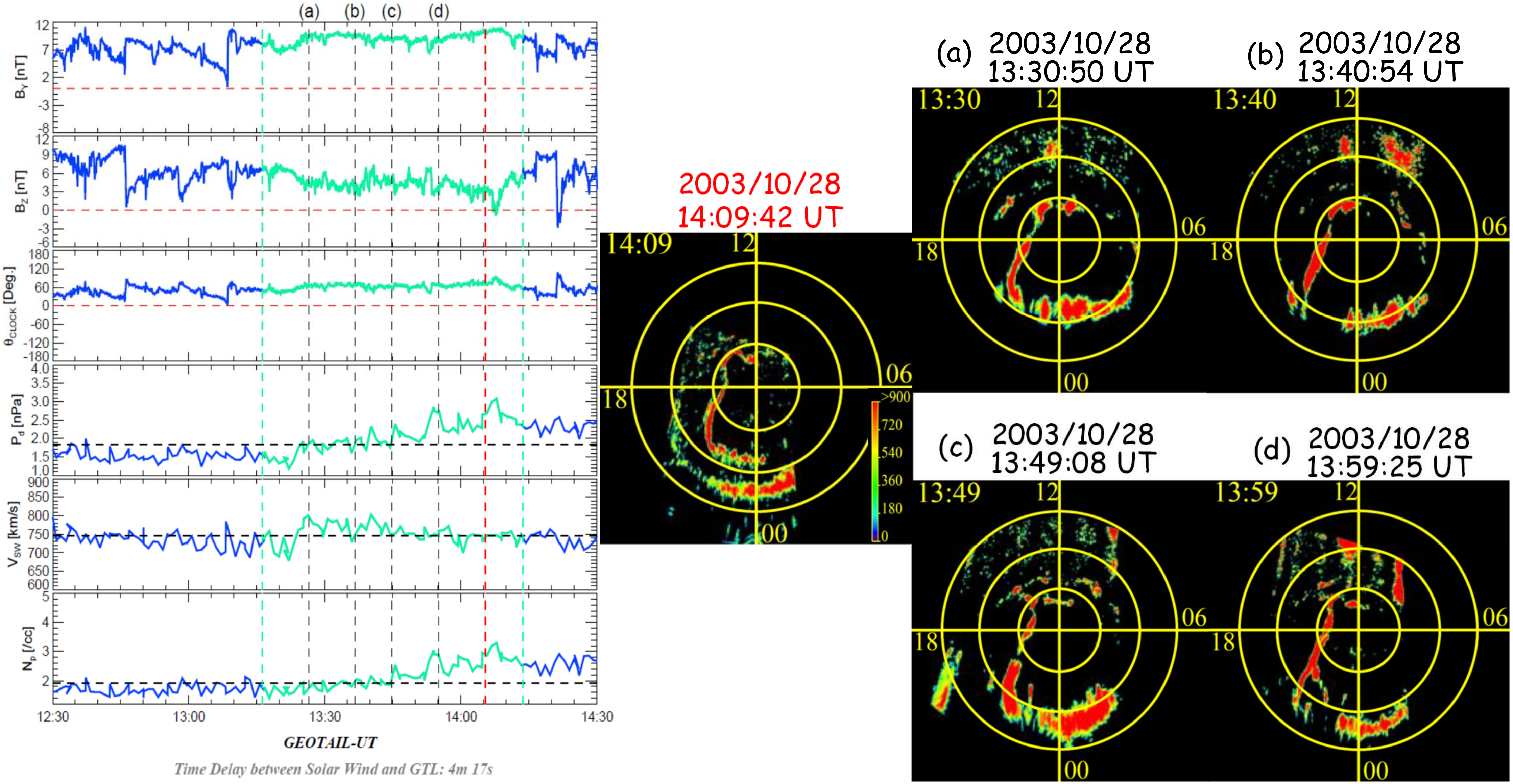

Figure S1. The 5 auroral imager snapshots of evolutional time sequence of the nightside distorted TPAs (right) and corresponding solar wind conditions (left) obtained from the OMNI solar wind database and the Geotail solar wind measurements are displayed. The "J"- and "L"-shaped TPA events observed on September 22nd, 2000 and November 5th, 2000 are shown in Figures S1A and S1B. Figures S1C and S1D display another "J"- and "L"-shaped TPA cases seen on December 31st, 2001 and October 28th, 2003, respectively. The plots of solar wind conditions show the IMF-B_y and -B_z components in GSM coordinates, IMF clock angle, calculated by $\tan^{-1}$(IMF-B_y/IMF-B_z), solar wind dynamic pressure ($P_d = m_p N_p V_{sw}^2$), when solar wind ion species are assumed as protons, solar wind velocity and number density, respectively. The nightside distorted TPA intervals are plotted with light green and also bracketed by two light green broken lines. The black vertical broken lines, labelled from (a) to (d), correspond to the solar wind conditions at the times when the IMAGE FUV-WIC data from (a) to (d) shown in right column were obtained. The times when IMAGE FUV-WIC detected the clear "J"- and "L"-shaped TPA cases (middle) are highlighted with red, and associated solar wind conditions are indicated with red vertical broken lines. The IMAGE FUV-WIC data plot formats from Figures S1A to S1D are the same as that of Figure 1. The time delay between the solar wind and spacecraft location is indicated below the panels in the Geotail observational cases.

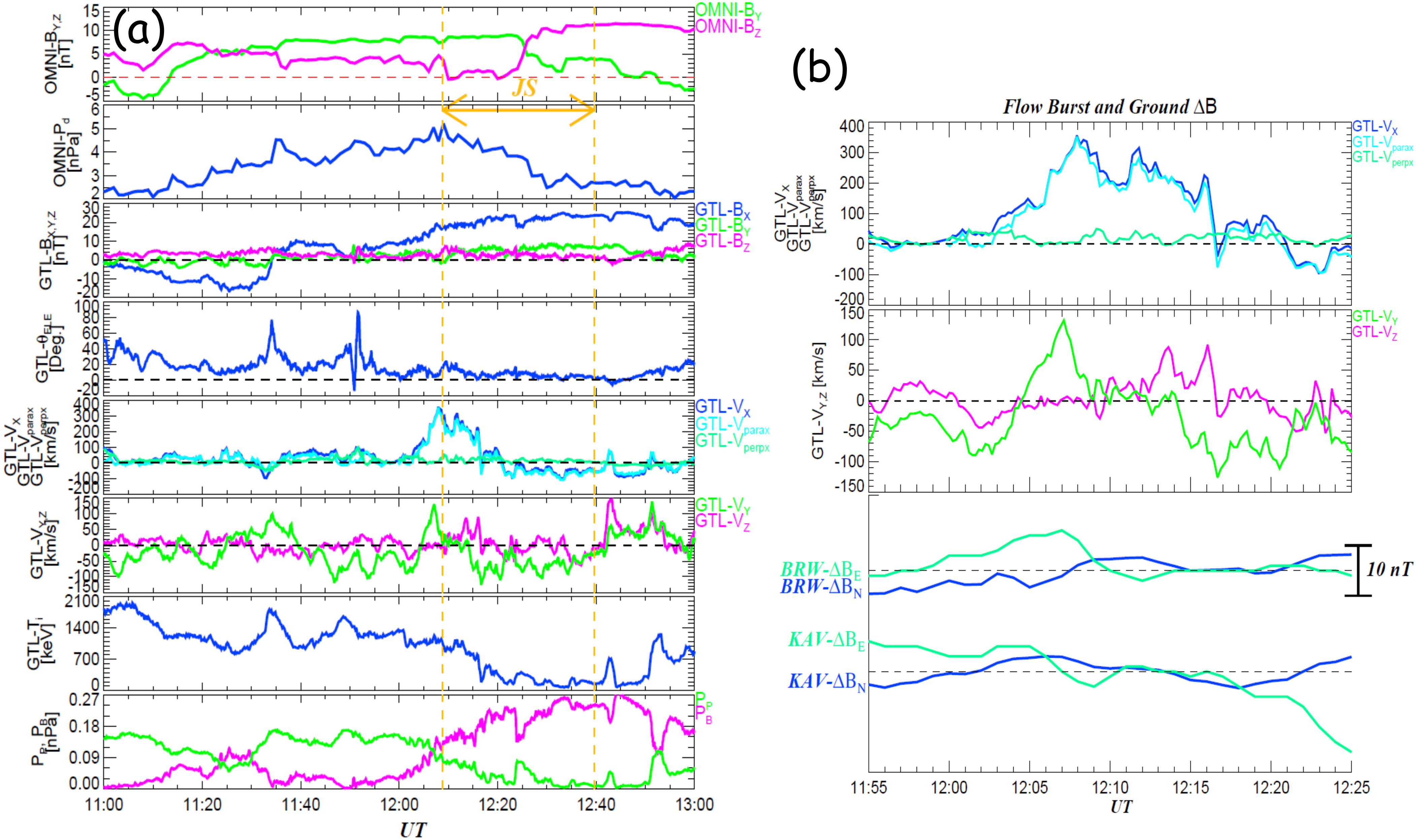

GTL Location during "J"-Shaped TPA in GSM: (-29.41, -9.71, 2.28)

Figure S2. The plots of in-situ dawnside magnetotail observation made by Geotail, corresponding solar wind conditions, and geomagnetic field variations at the observatories beneath and close to the proximity of the growth of the "J"-shape TPA seen on March 2^{nd}, 2002 are displayed. Panel (a) shows a summary plot of the solar wind conditions obtained from the OMNI database and Geotail dawnside magnetotail observations for 2 hours between 11:00 UT and 13: 00 UT. From top to bottom panels show the IMF-B_y and -B_z components in GSM coordinate system, solar wind dynamic pressure calculated by $m_p N_p V_{sw}^2$, where m_p, N_p, and V_{sw} indicate the mass of proton, number density and solar wind velocity, the three components of the dawnside magnetotail magnetic field in GSM, associated magnetic field elevation angle obtained by $B_z/\mathrm{sqrt}(B_x^2 + B_y^2)$, and GSM-X, -Y, and -Z plasma velocity components (V_x, V_y, V_z) in the dawnside magnetotail, respectively. In the panel of the V_x component, the X-components of plasma velocity parallel (V_{parax}) and perpendicular (V_{perpx}) to the local magnetic field lines are also superimposed, respectively. The time interval when the "J"-shaped TPA intensified is bracketed by two gold broken lines with a label "JS" and two-heads arrow. The Geotail location during the "J"-shaped TPA interval is shown in the bottom of the panels. Panel (b) shows the zoomed-up three plasma flow velocity components in GSM and X-components of the flow velocity components parallel and perpendicular to the local magnetic field lines, including the positive V_x enhancements which are suggestive of earthward plasma flow burst, and corresponding ground magnetic field variations observed at two representative magnetic observatories close to the "J"-shaped TPA. The ground magnetic field fluctuations are calculated by a subtraction of the magnetic field average during the presented interval from observed magnetic field data.

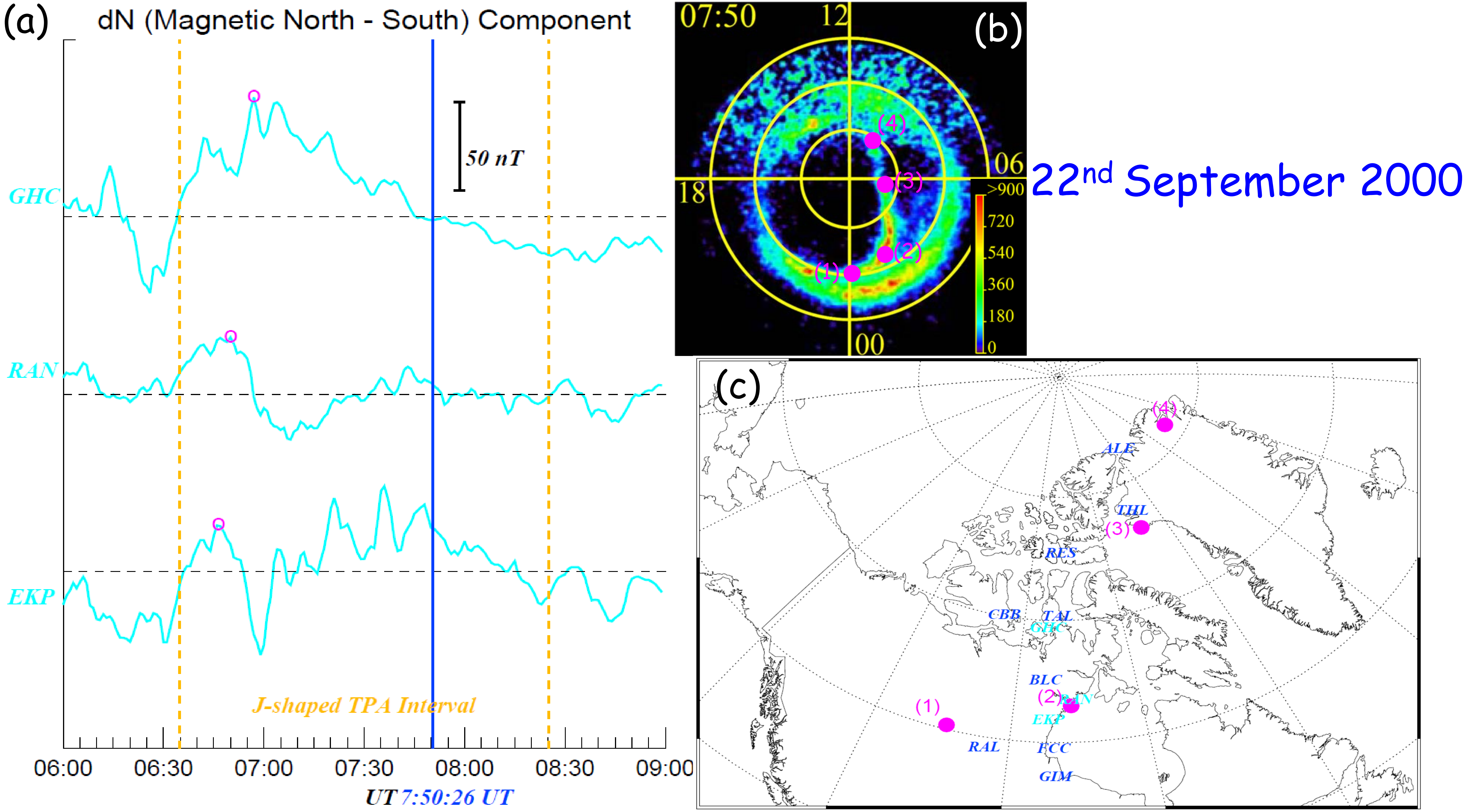

(a)
dN (Magnetic North - South) Component
50 nT
GHC
RAN
EKP
J-shaped TPA Interval
06:00
06:30
07:00
07:30
08:00
08:30
09:00
UT 7:50:26 UT
(b)
07:50
12
06
18
00
>900
720
540
360
180
0
(1)
(2)
(3)
(4)
22nd September 2000
(c)
ALE
THL
RES
CBB
TAL
GHC
BLC
RAN
EKP
RAL
FCC
GIM

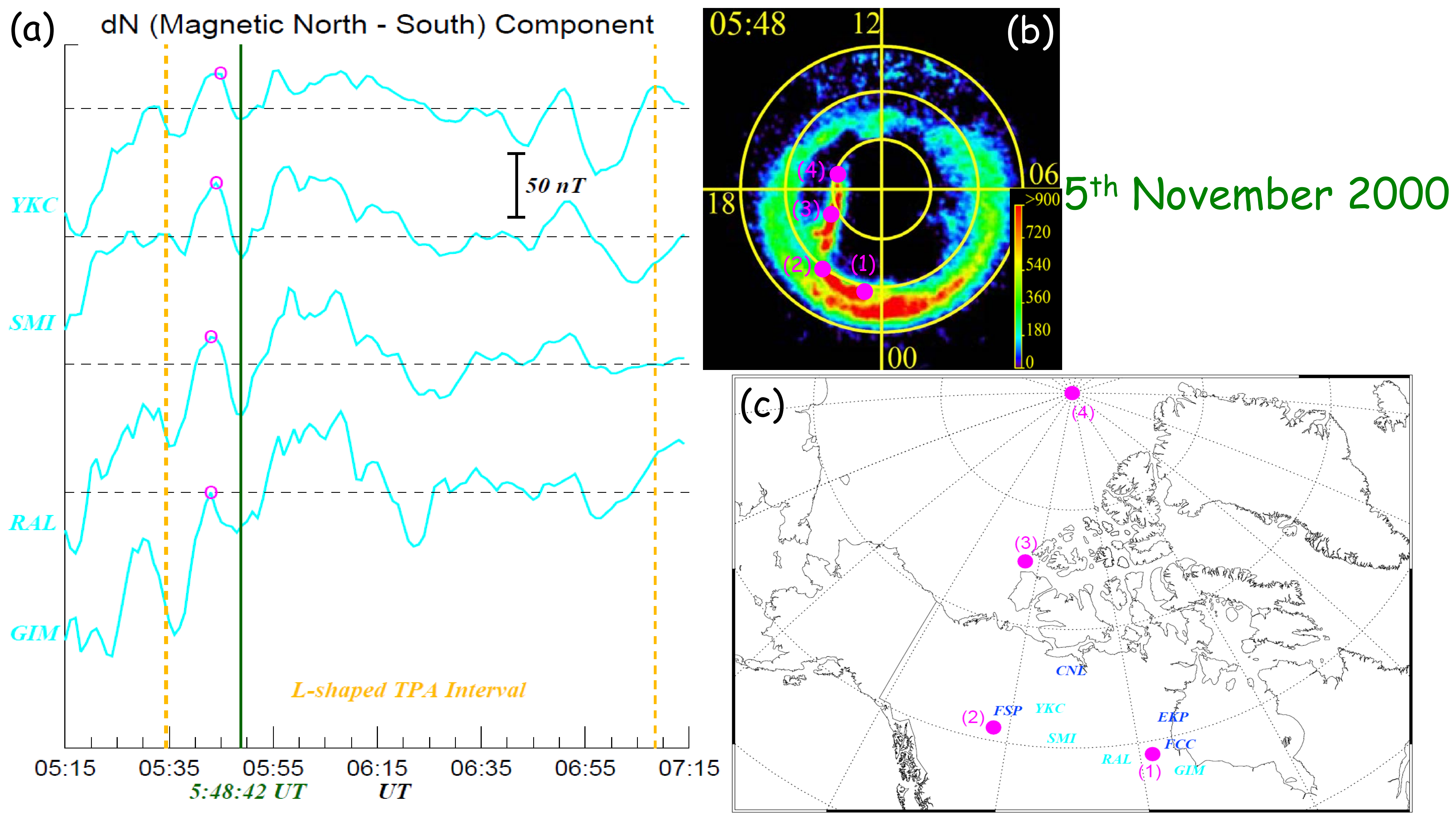

(a)
dN (Magnetic North - South) Component
50 nT
YKC
SMI
RAL
GIM
L-shaped TPA Interval
05:15
05:35
05:55
06:15
06:35
06:55
07:15
5:48:42 UT
UT
(b)
05:48
12
06
18
00
(1)
(2)
(3)
(4)
>900
720
540
360
180
0
5th November 2000
(c)
(1)
(2)
(3)
(4)
CNL
FSP
YKC
SMI
RAL
EKP
FCC
GIM

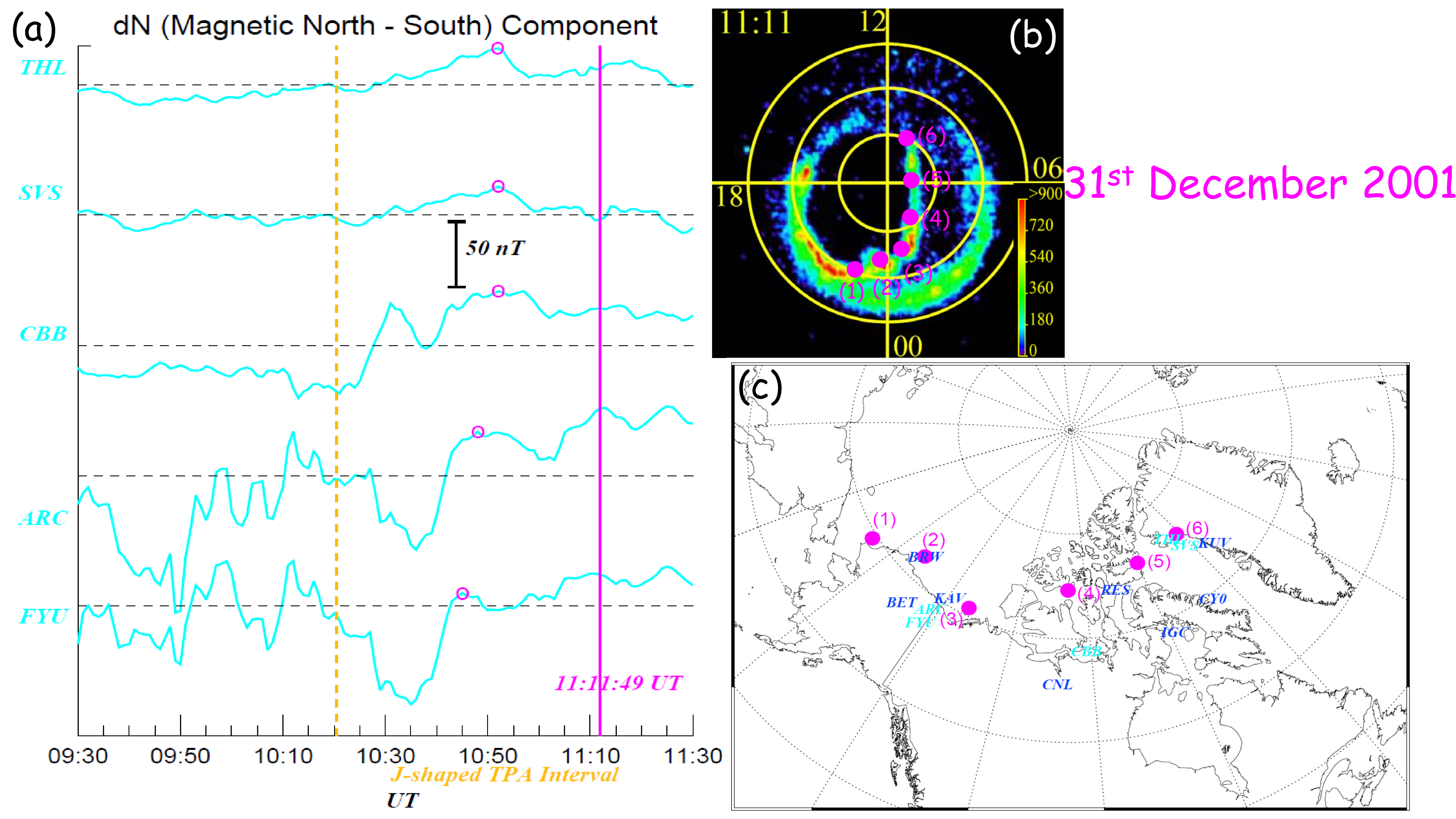
(a)
dN (Magnetic North - South) Component
THL
SVS
CBB
ARC
FYU
50 nT
11:11:49 UT
09:30
09:50
10:10
10:30
10:50
11:10
11:30
J-shaped TPA Interval
UT
(b)
11:11
12
06
18
00
(1)
(2)
(3)
(4)
(5)
(6)
>900
720
540
360
180
0
31st December 2001
(c)
(1)
(2)
(3)
(4)
(5)
(6)
BRW
BET
KAV
ARC
FYU
RES
KUV
CY0
IGC
CBB
CNL

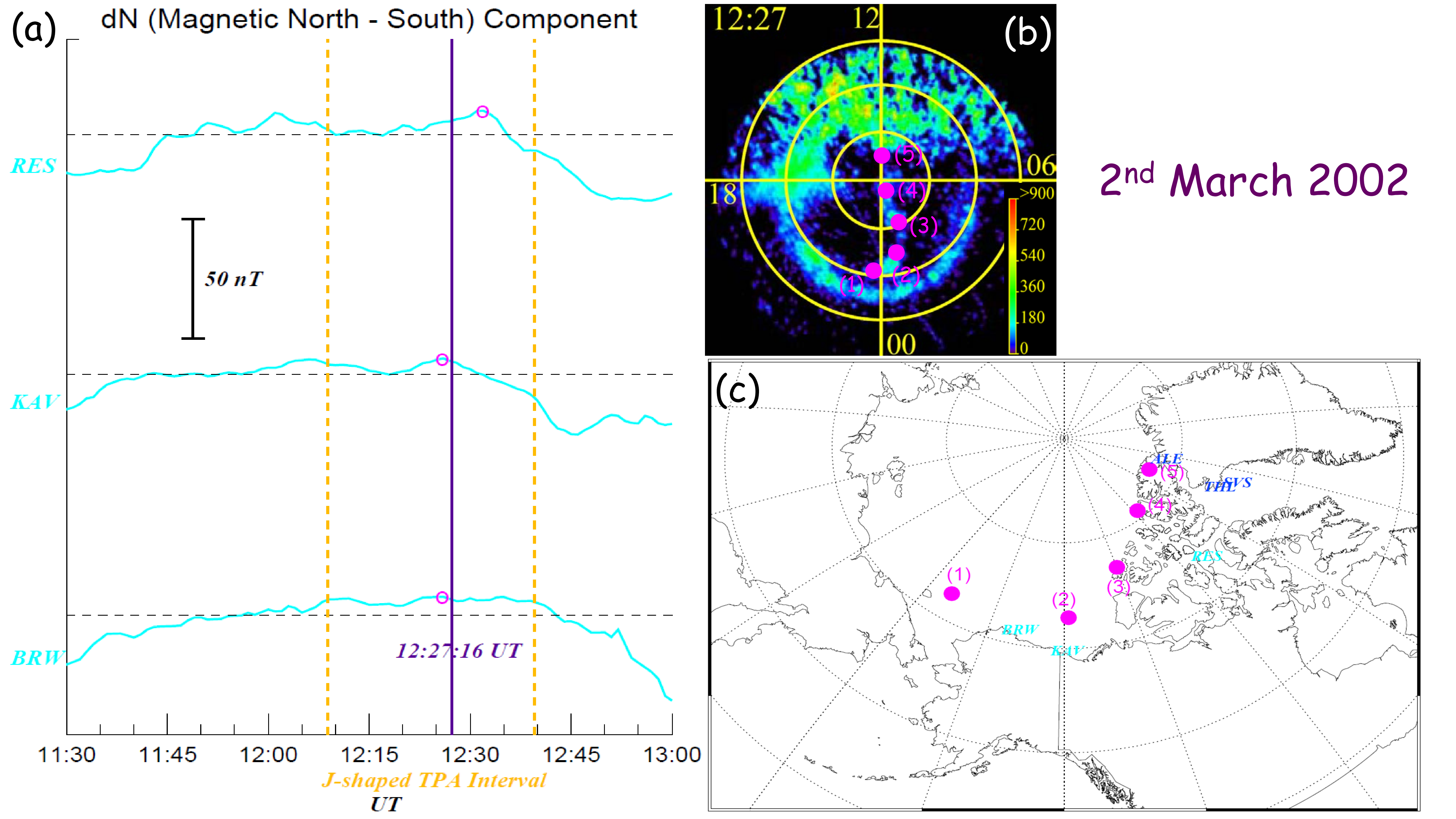

(a)
dN (Magnetic North - South) Component
RES
KAV
BRW
50 nT
12:27:16 UT
11:30
11:45
12:00
12:15
12:30
12:45
13:00
J-shaped TPA Interval
UT
(b)
12:27
12
06
18
00
>900
720
540
360
180
0
(1)
(2)
(3)
(4)
(5)
(c)
ALE
SVS
THL
RES
BRW
KAV
2nd March 2002

Figure S3. The plots of in-situ geomagnetic magnetic field variations beneath and in close proximity to the regions of growth of the 4 nightside distorted TPAs are displayed. Panels (a) to (c) show the magnetic field observational results at several ground magnetic observatories corresponding to the locations beneath or in close proximity to the growth regions of the nightside distorted TPAs. Several magenta points labelled with numbers in the IMAGE FUV-WIC plots (panel b) correspond to similarly labelled locations in geographical map (panel c). Panel (a) shows the plots of fluctuations in the local magnetic north-south magnetic field component (ΔB_N) at these observatories highlighted by cyan. The fluctuation component, which was obtained by the subtraction of average magnetic field over the time interval of interest from the observed magnetic field values, at each station is plotted upon their averages as indicated by horizontal grey broken lines, and its peak during the "J"- and "L"-shaped TPA intervals (indicated by one or two gold broken lines) is marked by magenta open circle. The plots are sorted in decreasing order of latitude. The magnetic field fluctuation component at the time of panel (b) is indicated by a horizontal solid line in the panel. The color code of the IMAGE FUV-WIC data is assigned according to ADU.

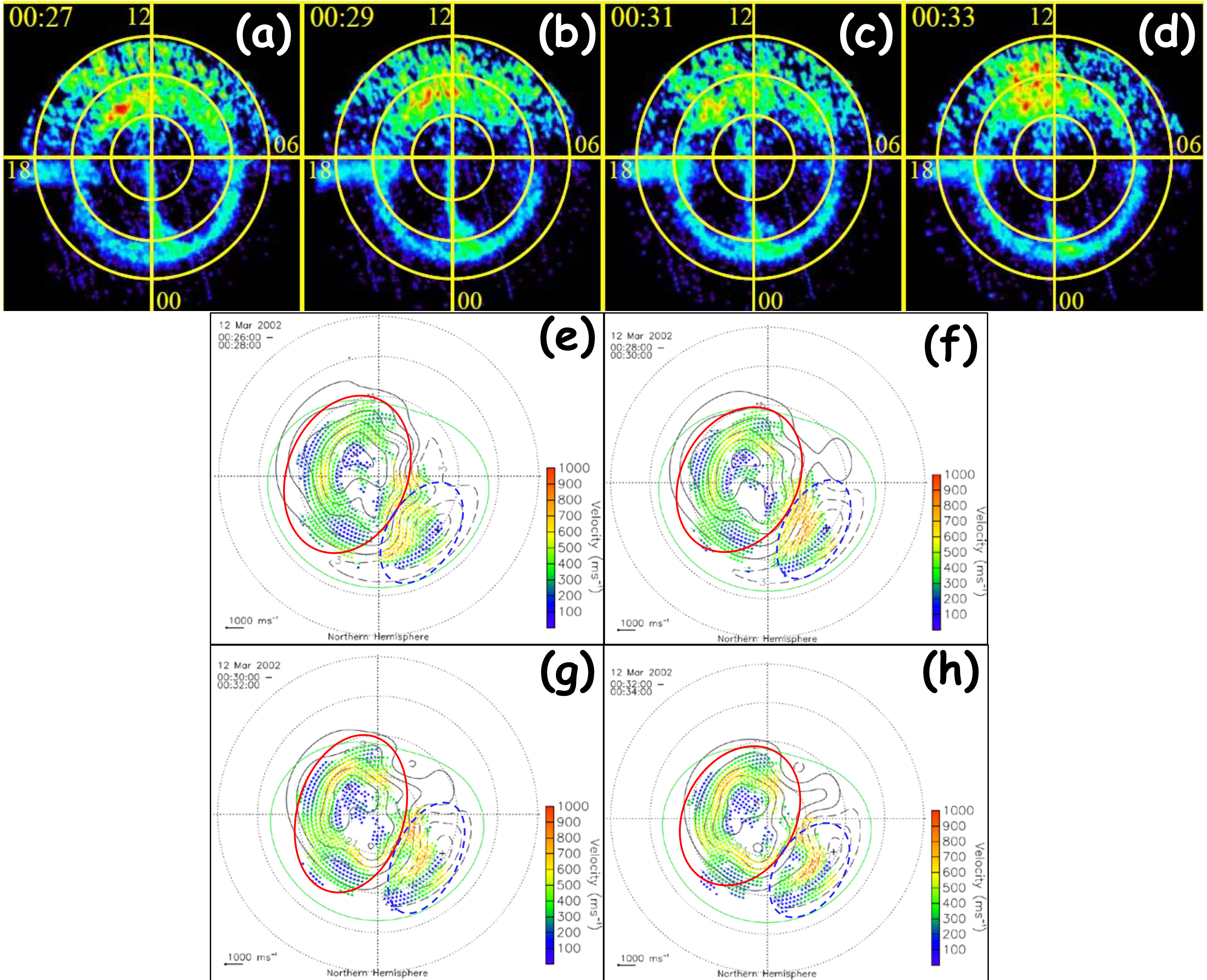

00:27
12
(a)
06
18
00
00:29
12
(b)
06
18
00
00:31
12
(c)
06
18
00
00:33
12
(d)
06
18
00
12 Mar 2002
00:26:00 –
00:28:00
(e)
1000
900
800
700
600
500
400
300
200
100
Velocity (ms-1)
1000 ms-1
Northern Hemisphere
12 Mar 2002
00:28:00 –
00:30:00
(f)
1000
900
800
700
600
500
400
300
200
100
Velocity (ms-1)
1000 ms-1
Northern Hemisphere
12 Mar 2002
00:30:00 –
00:32:00
(g)
1000
900
800
700
600
500
400
300
200
100
Velocity (ms-1)
1000 ms-1
Northern Hemisphere
12 Mar 2002
00:32:00 –
00:34:00
(h)
1000
900
800
700
600
500
400
300
200
100
Velocity (ms-1)
1000 ms-1
Northern Hemisphere

Figure S4. The 4 consecutive IMAGE FUV-WIC data during the "L"-shaped TPA interval from 00:27 UT to 00:33 UT on March 12^{th} 2002 (panels a to d), and corresponding SuperDARN radar data (panels e to h) are shown, respectively. During this time interval, the ionospheric current structure with a large-scale anti-clockwise vortex was seen in close proximity of the "L"-shaped TPA (as shown in panels a to d) in Figure 3, supporting that upward (from ionosphere to magnetotail) FACs occurred. Taking a look at associated plasma flow vectors detected by SuperDARN arrays, a large-scale clockwise plasma flow vortex was seen (highlighted with red ovals), being consistent with the occurrence of anti-clockwise vortex ionospheric currents which indicate the presence of upward FACs near the TPA, shown in Figure 3. In opposite dawnside sector, anti-clockwise plasma flow vortex (surrounded by blue broken line ovals) was seen, supporting that clockwise ionospheric currents, which are evidence for the occurrence of downward (from magnetotail to ionosphere) FACs.

Table S1. Fundamental information on the 9 nightside distorted TPA events used in this study, and values of key parameters on the associated magnetospheric conditions are summarized.

	Event Date	TPA Interval (UT)	Duration Interval (minutes)	Type of Nightside Distorted TPA	IMF-B_z Direction	IMF-B_y Direction	Average *AL*/*AU* [nT]	K_p	Ground-Based Observation	IMAGE N/S Hemisphere
I	2000/9/22	6:34:53 – 8:25:08	110	J	Northward	Dawnward	-40/80	2-	Yes (Data Used)	NH
II	2000/11/5	5:34:24 – 7:08:24	94	L	Northward	Duskward	-100/50	3+	Yes (Data Used)	NH
III	2000/12/27	23:31:42 – 00:33:05	63	J	Northward to Southward	Dawnward to Duskward	-18/23	2-	Yes (No Used) †1	NH
IV	2001/12/31	10:20:34 – 14:40:46	260	J	Northward	Dawnward	-25/90	1+	Yes (Data Used)	NH
V	2002/3/02	12:08:49 – 12:39:34	31	J	Northward	Duskward	-29/25	1+	Yes (Data Used)	NH
VI	2002/3/12	00:19:16 – 00:58:12	39	L	Northward	Duskward	-31/44	2+	Yes (Data Used)	NH
VII	2003/10/28	13:20:18 – 14:17:55	58	L	Northward	Duskward	-295/40	3-	Yes (No Used)†2	NH
VIII	2004/6/5	9:42:37 – 10:15:44	33	L	Northward to Southward	Dawnward	-25/90	2+	No	SH
IX	2005/6/1	11:28:38 – 12:14:28	46	J	Northward	Dawnward to Duskward	-58/25	2-	No	SH

†1 Neither peaks nor variations in geomagnetic field during the interval of the nightside distorted TPA were found.

†2 The clear peaks cannot be identified because of highly magnetic fluctuations during the interval of the nightside distorted TPA.

Table S2. The station code, geographical longitude (GEOLon), latitude (GEOLat), geomagnetic longitude (MLon), latitude (MLat), and station name are listed with the order from high- to low-latitudes in geographic coordinates (GEOLat). The GEOLon and GEOLat in each station is calculated based on the IGRF-2010 model, which can be downloaded from the SuperMAG website (http://supermag.jhuapl.edu/mag/). The magnetic field data obtained from these ground stations are used to draw the electric current vectors as shown in Figure 3.

Station Code	GEOLon [deg.]	GEOLat [deg.]	MLon [deg.]	MLat [deg.]	Station Name
ALE	297.50	82.50	86.95	87.14	Alert
THL	297.77	77.47	29.24	84.72	Qaanag
SVS	294.90	76.02	32/87	83.00	Savissivik
RES	265.11	74.69	-35.54	82.93	Resolute Bay
UPN	303.85	72.78	40.20	78.93	Upernavik
CY0	291.4	70.5	18.88	78.52	Clyde River
SCO	338.03	70.48	71.82	71.63	Ittoqqortoormiit
IGC	278.2	69.30	-5.39	78.43	Igloolik
GDH	306.47	69.25	39.39	75.25	Godhavn
ATU	306.43	67.93	38.19	73.99	Attu
STF	309.28	67.02	40.87	72.64	Kangerlussuaq
PGC	294.2	66.10	20.55	74.09	Pangnirtung
AMK	322.37	65.60	53.57	68.99	Tasiilaq
SKT	307.1	65.42	37.22	71.43	Maniitsoq
LRV	338.3	64.18	66.72	65.01	Leirvogur
GHB	308.27	64.17	37.85	69.98	Nuuk
HLL	339.44	63.77	67.40	64.41	Hella
IQA	291.48	63.75	15.58	72.21	Iqaluit
FHB	310.32	62.00	39.05	67.41	Paamiut